The applicability of G-BASE stream sediment geochemistry as a combined geological mapping, and prospective exploration tool for As-Co-Cu-Ni mineralisation across Cumbria, UK.

Adam Eskdale[1]; Sean C. Johnson[2*]; Amy Gough[1]

[1]Department of Earth Sciences, Royal Holloway University of London, UK
[2]Earth Science, University College Dublin, Belfield, Dublin 4, Ireland
*Current address – Rio Tinto Exploration, Reading, UK

Author Correspondence:

Email: Adam.Eskdale.2019@live.rhul.ac.uk;

Twitter: @EskdaleAdam

Keywords: G-BASE, stream sediment geochemistry, cobalt, mineral exploration, Lake District, critical metals

This manuscript is a non-peer reviewed preprint submitted to EarthArXiv. The same copy has been submitted for peer review and publication with the Journal of Geochemical Exploration (Elsevier). Currently in-review.

1 Abstract

Stream sediment geochemistry is a useful tool to analyse the geochemistry of the local geology within the source catchment area. This has significant applicability within the field of mineral exploration where understanding regional lithological geochemistry is needed, facilitating the identification of critical metal deposits. Successful identification of these deposits is essential to help tackle the deficit of these metals supply chains, especially for cobalt. This is in order to meet future carbon-neutral technological demand as part of global initiatives towards a more environmentally sustainable society.

We make use of the UK Geochemical Baseline Survey of the Environment (G-BASE) dataset to demonstrate that stream sediment geochemical data has the potential to be used as a useful tool for isolating potential Energy Critical Elements (ECEs) in host rocks across the UK Lake District. We reduced the dimensionality of the G-BASE stream sediment data, creating geochemical maps that identify a combination of volcanic, sedimentary, and plutonic lithologies lining up geological boundaries from established 50k scale geological maps of the area. This was conducted through a combined statistical and mapping approach within QGIS and ioGAS.

Furthermore, we identified average ore metal concentrations (Ag, As, Bi, Co, Cu, Mo, Ni, Sn, Zn) for the Skiddaw Group and the Borrowdale Volcanic Group, two established host groups for As-Co-Cu-Ni mineralisation. Average concentrations of Co in the Skiddaw have been modelled to be 63.26 ppm, and in the Borrowdale volcanics to be 26.86 ppm. These values, combined with As, Cu, and Ni modelled concentrations, and other available exploration-related data (structural maps, underlying batholith topography, mining history etc.) have allowed us to identify 10 prospective areas of interest for possible As-Co-Cu-Ni mineralisation across these two lithological groups. This workflow has strong applicability within critical metal exploration in other, more prospective regions across the globe.

2 Introduction

2.1 Critical Metal Necessity

As defined in the 2015 Paris Climate Agreement, the goal of societal carbon-neutrality by minimum 2050 requires an increased global production of Plug-in Hybrid Electric Vehicles (PHEV), critical to this being the supply of Energy Critical Elements (ECEs) such as Ag, Al, Cr, Co, Cu, Fe, In, Li, Mn, Mo, Nd, Ni, Pb, V, and Zn (Darton Commodities Ltd. 2020; Hund et al. 2020; Dehaine et al. 2021; Tabelin et al. 2021). Cobalt (Co), in particular, is used in various industries related to the production of renewable technologies including PHEV, Li-Co batteries, and high-strength magnets (Alves et al. 2018; Dehaine et al. 2021; Solferino et al. 2021). There is a current monopolisation of global supplies with 69 % of 2020 global Co mining from the Democratic Republic of Congo (DRC) (Gulley. 2021). The majority of cobalt production is in the form of by-products, associated with copper and nickel mining (Hitzman et al. 2017) with primary Co deposits both rare and less understood in comparison to other critical metals (Ag, Au, Cu, PGEs). With the projected global demand for Co set to exceed 460 % of its current value by 2030 (Alves et al. 2018; Nguyen et al. 2021), these combined factors mean that faster, more effective exploration for Co has never been more critical.

2.2 Geochemical Mapping as a Tool for Mineral Exploration

Quantitative, geochemical investigations using stream sediment, stream water, and soil data as a geological mapping tool have been successfully applied to mineral exploration. Although traditional geological mapping frameworks should not be replaced (i.e., on-the-ground observations, geological mapping, methodical sampling etc.), tools that can be combined with these workflows to provide rapid identification and exploitation of base, precious and critical metal deposits could be a crucial part of the future of Co mineral exploration, especially useful when time is often a constraining factor. Rapidly attaining a detailed understanding of regional and local scale geological formations, features and structures is key for future deposits to be found sooner. In Ireland, the TELLUS project used stream sediments and soil geochemistries

as a predictive tool for geological mapping rock types, and stream water data as a mineralisation pathfinder tool by mapping concentrations for base-metals and gold (Steiner. 2018; Gallagher et al. 2022). In Brazil, the 'Itacaiunas Basin Geochemical Mapping and Background Project' (ItacGMBP) regional mapping programme has been used for mineral exploration and to assess environmental contamination (Salamao et al. 2020). And, west-central Nigeria the 'Nigerian Geochemical Mapping Technical Assistance Programme' (NGMTAP) project identified placer deposits related to Au, REE, Ta, Nb and U (Lapworth et al. 2012). However, further work can help to refine these methodologies.

UK-based mineral exploration is relevant to the growing interest of critical mineral supplies (Walton et al. 2021). The Geochemical Baseline Survey of the Environment (G-BASE) run by the British Geological Survey (BGS) contains data on stream sediment, water and soil geochemistry. It also provides the potential to aid in developing metallogenic models and to identify mineralisation by providing a regional geospatial lithogeochemical database. This dataset has been successfully applied in SW England (Kirkwood et al. 2016a, 2016b) and proven useful for identifying regional distinct areas of geology in Devon-Cornwall. The BGS has previously used G-BASE in Cumbria (British Geological Survey, 1992, Rawlins et al. 2012; Everett et al. 2019), to highlight areas of environmentally damaging elements and anomalies of elements and metals with economic value. Further use of this dataset focused on specific tasks, such as mapping U anomalies, and using the soil chemistry data to geochemically map Pleistocene deposits (Chenery et al. 2002; Scheib et al. 2007; Johnson et al. 2011). Here, the stream sediment geochemistry offers insight into regional geochemistry and mineralisation as it can be linked to the source rock lithology, and therefore potential sites for mineralisation of ECEs can be identified. Although using stream sediment geochemistry as a geological mapping tool is not novel, the use of G-BASE for mapping potential As-Co-Cu-Ni vein mineralisation in Cumbria is. This takes the original methodology and applies it in a unique manner for mineral exploration purposes.

2.3 A Brief Geological Setting of Cumbria

The geology of Cumbria (Figure 1) is predominantly Ordovician (500 Ma) to Jurassic (200 Ma) in age (Moseley, 1978; Stephenson et al., 1999). Around 480 Ma the Avalonia and Gondwana tectonic plates separated, leading to the closure of the Iapetus Ocean. Around 400 Ma Avalonia and Laurentia collided leading to the Caledonian (Acadian) Orogeny (Torsvik et al., 1996; Pharaoh, 1999). The oldest subdivision from these events is the Lower Ordovician (485 - 470 Ma) Skiddaw Group (SKD) (previously referred to as the Skiddaw Slates) comprised mostly of mudstones, siltstones, sandstones, and sporadic greywackes outcropping across the Northern Fells of the Lake District, and to a smaller extent in the Southern Fells as the Black Combe inlier (Cameron et al., 1993; Cooper et al. 1995; Lott and Parry, 2017). The Eycott Volcanic Group (EVG) formed contemporaneously with the upper Skiddaw Group during the Middle Ordovician, exposed in the Northern Fells as interbedded basaltic-rhyolitic layers (Moseley, 1978). Following this, during the Upper Ordovician, the Borrowdale Volcanic Group (BVG) formed and comprises interbedded ash-fall tuffs, ignimbrites, and andesitic lavas mostly the product of calc-alkaline, subaerial volcanism (Branney and Soper, 1988; Scoon, 2021).

[Figure 1 here]

During the Upper Ordovician, a major granite-granodiorite batholith was emplaced underneath the Lake District and outcrops almost exclusively in the Skiddaw Group and Borrowdale Volcanic Group. The earliest outcrops are the Ennerdale pluton (452 ± 4 Ma) outcropping in both the SKD and BVG (Figure 1), and the Eskdale pluton (450 ± 3 Ma) in the BVG (Hughes et al. 1996; Stone et al. 2010). These plutons vary slightly in composition, with the Ennerdale being having a more granodiorite composition and the Eskdale being more granitic; however, both are thought to originate from the Iapetus-closure, subduction environment which formed the underlying batholith (Bott. 1974; Millward et al. 1978; O'Brien et al. 1985; Cameron et al. 1993) and are collectively known as the Lake District Ordovician Felsic Plutonic Suite (OFPS). The Lake District Ordovician Mafic Plutonic Suite (OMPS) and Ordovician Minor Intrusion

Suite (OMIS) also formed in this period (Figure 1). Subsequent waning in volcanism and regional subsidence let to a marine transgression marked by an unconformable boundary and the Windermere Supergroup (WSG) – a series of Upper Ordovician limestones and mudstones overlain by Silurian interbedded sandstones and siltstones (450 - 400 Ma) (Moseley, 1978; Branney and Soper, 1988; Cameron et al., 1993).

During the Lower Devonian further granite emplacement occurred, just prior to the Acadian deformation, outcropping as the Shap (404 ± 1 Ma) and Skiddaw (399 ± 1 Ma) granites (Figure 1) (Woodcock et al. 2019). These formed separate to the aforementioned batholith, during the Caledonian orogeny and are known as the Northern England Devonian Plutonic Suite (DPS) and Lake District Devonian Minor Intrusion Suite (DMIS).

Following the Caledonian orogeny N-S orientated lithospheric extension led to rift basins forming across the Cumbria - Northern UK region (Stephenson et al., 1999). The grabens were dominated by shallow-environment, Carboniferous Limestone (CL) carbonate reefs. Tectonic activity waned by the middle Mississippian, the last intrusive activity being the dolerites and microgabbro of the North Britain Late-Carboniferous Tholeiitic Suite (LCTS), and deposition followed predominantly cyclically as sandstones, mudstones, and siltstones. These are referred to partially as the Millstone Grit Group (MGG) (Stephenson et al. 1999). Erosional features along fault systems during the Devonian then led to deposition of the Mell Fell Conglomerate (MFC) (Capewell. 1955).

The Variscan Orogeny, which started prior to the Visean, is expressed across the Lake District through overturned beds and reactivation of syn-depositional, extensional faults from the N-S compression (Moseley, 1978; Tait et al., 1997). The youngest lithological groups in Cumbria are the Permian – Jurassic sandstones and mudstones (PS), the Sherwood Sandstone Group (SSG), and Mercia Mudstone Group (MMG), predominantly exposed in Northern and Eastern Cumbria (Figure 1).

2.3.1 Mineralisation

Mineralisation is varied across Cumbria but is typically categorised into Baryte, Co, Cu, Graphite, Haematite, Sb, Pb (+Zn) and W occurring as a mixture of skarns, greisens, sedimentary ores, and mineralised veins (Stanley & Vaughan. 1982a, 1982b; Ixer et al. 1979; Solferino et al. 2021). The hypogene mineralisation episodes are believed to have occurred between the Middle Ordovician (Dapingian Stage - 470 Ma) and the Lower Jurassic (Hettangian - 200 Ma). Key periods of economic mineralisation are: 1) chalcopyrite-pyrite-arsenopyrite veins deposited in the Lower Devonian; 2) galena-sphalerite-baryte veins from the Early Carboniferous (Stanley and Vaughan, 1982a). Mineralisation of these types was historically mined throughout the Lake District. Cobalt mineralisation is known to be concentrated within some of the Devonian 'As-Cu-Fe' series (Russell, 1925; Ixer et al., 1979; Stanley and Vaughan, 1982a; Cooper et al., 1988), compositionally similar to the 'Five-Element Type' As-Co-Cu-Ni composition (Kissin. 1992). The SKD and BVG are the main host groups, with vein-type As-Co-Cu-Ni mineralisation at Scar Crags and Dale Head North (Solferino et al. 2021), and minor Co-occurrences noted at Seathwaite and Ulpha (Ixer et al. 1979; Stanley & Criddle. 1979; Stanley & Vaughan. 1980, 1982a; Eskdale et al. 2021). These ores are thought to be emplaced between 390 - 370 Ma (Stanley and Vaughan. 1982a). Copper mineralisation is the most widespread in the region, and there is significant data collected regarding its genesis compared to that of the other commodities. Since Co is associated with chalcopyrite-bearing veins, Cu is a useful analogue to track potential further cobalt mineralisation as they most likely emplaced during the same event.

The Lake District As-Co-Cu-Ni mineralisation is associated with the emplacement of the aforementioned underlying batholith (Firman & Lee. 1986; Stone et al. 2010), with the Scar Crags mineralisation relating to slightly shallower batholith topography and Dale Head North to slightly higher (Solferino et al. 2021). The ores were formed most likely from a mixing of magmatic fluids, originated from the intrusive body, and meteoric fluids that circulated through the SKD and BVG (Stanley and Vaughan. 1982a; Solferino et al. 2021). Numerous, regional

scale structures were formed across the Lake District from the Caledonian Orogeny. These faults are most likely the main migration network that the hydrothermal fluids followed when emplacing the Devonian ‘As-Co-Cu-Ni’ veins (Dagger, 1977; Stanley and Vaughan. 1982a). The majority of localities bearing these veins are located above the faulted-boundaries and flanks of the underlying batholith (Dagger, 1977; Stanley and Vaughan, 1982a). As all of the ‘As-Co-Cu-Ni’ ore is found in veins with orientations reflecting that of the batholith roof region, trending ENE or EW, this is further evidence the ore-forming fluids were at least partially derived from the batholith (Firman. 1978; Stanley and Vaughan, 1982a). However, not all Cu-Fe-As mineralisation is found on the ridges and not all these veins follow this orientation, indicating there is yet still another control on the emplacement of Co to be understood.

The Lake District is therefore a strong proxy for typical economic ore-forming settings, with As-Co-Cu-Ni minerals derived from oceanic-arc, subduction-related magmas and mixing of magmatic and meteoric fluids into fault-controlled and oriented vein structures (Strens 1962’ Firman. 1978; Firman & Lee. 1986; Millward et al. 1999).

3 Methods

3.1 Regional Geochemistry: G-BASE Dataset

The G-BASE stream sediment, soil, and water geochemistry datasets (Johnson et al. 2005) contain data across the whole of the UK, with this study accessing the data for Cumbria. A total of 3974 stream sediment and water samples were collected for 56 different elements (Figure 2). Full details on the sampling and the QAQC for the dataset are found in Lister and Johnson (2005). This data was organised in MS Excel first to remove invalid or NULL data and to categorise the samples before being processed within ioGAS-64 geochemical software (QAQC, statistical analysis, initial interpretations) and projected geospatially within QGIS. All elements were converted to common units (ppm) and any elements with multiple collection methods were combined into one column to be used as a whole (Figure 2).

[Figure 2 here]

3.2 Geological Classification and Test Data

To establish the success of the geological mapping, we compared the results to the BGS 50k geological map geological boundaries. Geological formations and groups to test against were chosen based on the well-documented geological boundaries (Figure 1) in accordance with the BGS 50k scale geological maps of Cumbria (Brown, 1980). A spatial-join (within QGIS) was conducted between this map and the G-BASE stream sediment data, creating an average element value (ppm) per formation and group. This was restricted to those lithologies that had significant enough surface outcrop overlapping with G-BASE data points (see Appendix A, Figure A1). Three formations from the BGS 50k geological map have been excluded due to this, specifically the Upper Old Red Sandstone Formation, Carboniferous-Permian Dykes, and the North Britain Siluro-Devonian Calc-Alkaline suite.

3.3 Selection of Elements based on Mobility and Data Quality

Certain factors needed to be considered when using stream sediment data for the purposes of this study, the mobility of elements within the environment being key. Contrary to previous studies that removed hydrothermal elements from the data pre-analysis (Kirkwood 2016b), this study retained them as these concentrations are critical to highlighting possible ore anomalies.

[Table 1 here]

Elements that had significant data missing or no measurable concentration (0 ppm) were removed (Table 1). From a total of 56 measured elements, 21 were removed from the dataset. Following this, Cd was excluded due to significant amounts of questionable quality values. Bismuth also had a significant amount of questionable quality data but was kept due to its importance in recognising vein-type ores. A total of 34 elements were accepted and used in this study. It is also worth noting within the accepted elements, As data was collected using a

combination of XRF and AAS whilst all other elements were measured using ‘Direct Reading Optical Emission Spectroscopy’ (DCOES). In studies with similar methodology to this one (Kirkwood et al., 2016b), a similar elemental exclusion process was conducted to the G-BASE dataset with successful results.

3.4 Statistical Analysis

3.4.1 Empirical Analysis

Individual element anomalies were defined using progressive percentile brackets across the individual element datasets, categorised by observations of the element concentrations on a probability plot following a traditional statistics approach to exploration (Zuo et al. 2021). There is a variety of interpolation-based mapping styles that can be used to present anomaly-based data, for this study we used point-style data.

3.4.2 Principal Component Analysis

Principal component analysis (PCA) is a technique typically used for dimensionality reduction of large datasets. The use of PCA for interpreting geochemical data, especially within the field of mineral exploration, is a well-established multivariate technique and numerous workflows exist for identifying different rock types or mineral vectoring using host-rock bulk geochemistry data (Lawie, 2010; Gazley et al., 2015; Zuo et al. 2021).

Our PCA was conducted in ioGAS and used 3729 of the total 3978 available data points, therefore should reflect the entire dataset relatively well. Of the 34 available elements, 27 were used in the PCA, with 7 elements requiring exclusion at this stage due to the presence of NULL or 0 values. In contrast to the previous exclusion process, any NULL or 0 values here impact the PCA results due to the need for ‘closed’ compositions (Grunsky. 2010). An automatic unit conversion was used (although not strictly necessary as all elements were in ppm upon input to ioGAS), before then being scaled to the Z-score (standard deviation) to allow comparison between elements of different logarithmic scales (e.g., oxides will have

several logarithmically higher concentrations than trace metals). The data was also transformed using a central log ratio (CLR) prior to analysis. Conducting this analysis without performing a CLR first results in untransformed data that is not technically ‘closed’ and gives less of a defined spread (Aitchison. 1982, 1986; Grunsky. 2010; Grunsky et al. 2020).

3.4.2.1 Selection of principal components

The number of principal components selected for further use was established using a scree plot: 8 components were used as PC 1-8 have eigenvalues >1, following the Kaiser criterion for selection (Kaiser. 1960), cumulatively representing 74.46 % of the total data. It is typically accepted that components with eigenvalues < 1 are not useful when using this selection method as the eigenvalue needs to be >1 to fully represent a single variable. When projected onto a map, principal components 9-12 represented very mixed data, cutting across numerous lithological formations and so these principal components were excluded from the K-means analysis. Kaiser criterion was selected rather than choosing the ‘elbow’ of the scree plot (PC1 – 6) as geological formations may still have been represented in PC7 and 8, despite having a relatively lower eigenvalue.

3.4.3 K-means Cluster

The resolution of the K-means clustering results for representing geological linework varies due to the random-selection of the K value during the analysis. Each repetition of the analysis on the same data created slightly different cluster shapes depending on what random data point was chosen as the K value to base the clusters on; however, after several experimental repetitions it is deemed not to have a significantly detrimental impact on the overall results. Nine different analyses were conducted, three using PC1-6 as the input with max 5, 6, then 7 clusters, 3 using PC1-8 with max 5, 6, then 7 clusters, then 3 using PC1-12 with max 5, 6, then 7 clusters. Refer to Appendix C, Figure C1 for these experiment results. A total of 245 data points were excluded during the analysis from the final clustering results used in this study.

4 Results

4.1 Geological Mapping: Empirical Evidence for Lithology and Ore Identification

Anomalies of single elements in sediments in the sink can be linked to potential source geology, especially major oxides (Figure 3) which form a staple part of most lithologies (e.g. Fe, Si and Al are major components in shales, or Ca and Si in carbonates (Turekian & Wedepohl. 1961)) and ore metals which can indicate hosts or concentrations indicative of different types of mineralisation, such as As-Co-Cu-Ni veins (Figure 4).

4.1.1 Oxides

Calcium and Si are concentrated highest in the Carboniferous Limestone (CL), particularly in the northern and south-eastern outcrops (Figure 3A). The higher concentrations of Ca (> 20,000 ppm) overlap slightly with the Coal Measures (CM), whilst the higher concentrations of Si (> 36,000 ppm) overlap more so with the Permian sediments (PS) (Figure 3E). Manganese, Mg, Ti, and Fe all appear to concentrate highest within the Skiddaw Group (SKD), Borrowdale Volcanic Group (BVG) and Windermere Supergroup (WSG) with notable clustering around the Shap granite along the BVG – WSG boundary (Figure 3B, 3C, 3D, 3E). There is particular clustering of Mn and Fe just outside the boundary of the Eskdale granite, in the South-West BVG. Magnesium clusters more so around the northern Ennerdale granite – BVG boundary with minor clusters (> 17,000 ppm) throughout the WSG and CL (Figure 3D). High Ti concentrations (> 7, 000 ppm) cluster atop the Black Comb inlier and along the boundary between the BVG and WSG, with higher concentrations atop the volcanics compared to the sediments (Figure 4F). There are very sporadic points of higher Fe, Mn, Mg and Ti concentrations noted in the CL, with some Fe-Mg also sporadic in the Sherwood Sandstone (SSG).

[Figure 3 here]

4.1.2 Ore Metals

High concentrations of As (> 300 ppm) and Cu (> 120 ppm) are noted around the geological boundaries of the EVG and DMIS (Figure 4A, 4D). The higher values of Cu cover more surface area elsewhere than the As, across the SKD and BVG. Minor clusters of Bi are also noted in similar areas, near the Ennerdale and Eskdale granite boundaries (Figure 4B).

The highest concentrations of Co (> 100 ppm) are spread across the SKD and BVG, typically proximal to the Eskdale, Ennerdale and Shap granites (Figure 4C). Clusters of Co (60 – 100 ppm) are noted with As, Cu, Bi, and Ni around the EVG, and Co-Ni anomalies around the Shap granite (Figure 4E). Cobalt has relatively lower concentrations in the WSG whilst in contrast, Ni is noted almost exclusively in the WSG, SKD and CL with only a few exceptions in the BVG. It is worth noting that medium concentrations (green) of As, Bi, Co, and Ni are noted to overlap with the eastern parts of the CL, but not the sections dividing the SSG from the SKD-BVG-WSG.

Concentrations of Sn are the most sporadic of the ore metals (Figure 4F). Higher concentrations (> 50 ppm) are mostly noted in the BVG and Eskdale granite, and minorly in the SKD, WSG, SSG, and CL.

[Figure 4 here]

Overall, empirical evidence alone is not sufficient to identify clear lithological boundaries or smaller-scale mineralisation – only estimate at particular lithological boundaries and identify large areas of ore-associated metal concentrations. Further disaggregation of boundaries and identification of possible ore mineralisation requires a more unsupervised analytical approach using multivariate statistical techniques.

4.2 Geological Mapping: Unsupervised Analytical Approach

4.2.1 Principal Component Mapping

Established geological boundaries have been identified by using the first 6 principal components from a PCA, projecting them onto a map with the 50k geological linework overlain and combining them to create clearer spatial context in relation to the geology. This is shown using standard reg-green-blue (RGB) mapping (Figure 5). For individual PCA maps refer to Appendix B.

[Figure 5 here]

Overall PCs 1-3 represent 46.88 % of the total geochemical data (Figure 5). The geological boundaries across the volcano-sedimentary lithologies (SKD, BVG, and WSG) are the highest resolution. The BVG and hosted intrusives (OMIS, OMPS, and OFPS) are mapped out by PC2, and the SKD and WSG sediments by PC3. The remaining Carboniferous - Jurassic groups are then represented indistinguishably by PC1.

Positive values of PC1 are contributed by Si, Zr, U, Cr, La, Ti, and Sr in descending order of eigenvalue, concentrated within the CL, SSG, and CM. This draws a clear boundary against the SKD, BVG and WSG. Negatively contributing elements to the PC1 axis are Mn, Zn, Pb, and Co in ascending order of eigenvalue (Figure 5). These appear concentrated within the SKD and BVG, and to a lesser extent in the WSG and CL. The PC1 axis therefore distinguishes rock types with sandstones-, carbonate-based lithologies on the positive axis to more shale-, volcanic-based lithologies on the negative axis. Principal component 2 reflects 14 % of the overall data, represented by positive contributions of Rb, Ga, K, Be, V, Ti, Mg and Al in descending order of eigenvalue (Figure 5). Anomalously higher PC2 values are concentrated within the Ennerdale granite, high values contained mostly within the BVG, and mid-range values in the WSG. Negative PC2 values appear to concentrate primarily within the CL, minorly overlapping into the SSG and PS dominated by Ca and Sr. This component reflects mostly volcanic compositions at the positive end but does seem to overlap with felsic

and shale lithologies slightly (green tinges within OFPS, SKD and WSG boundaries). The negative axis appears to represent carbonates relatively well, similar to the negative PC1 values. It is also worth noting combined PC1-2 (yellow) on the Eskdale granite, most likely due to the high contribution of U, a typical endmember component for felsic granites (Turekian & Wedepohl. 1961). Principal component 3 reflects higher concentrations of Ni, Cr, V, and Mg in descending order of eigenvalue (Figure 5), representing 9.28 % of the total data. Highest PC3 values in these data points are contained within the eastern WSG, northern CL and across the SKD. The negative end of the axis, primarily contributed to by Y, La, Pb, and Be is sporadic across the region, indicating no relationship with a particular lithology.

Principal components 4-6 represent less data than PC1-3 (17.5 %) but draw attention to smaller scale geological features (Figure 5). Principal component 4 represents 7.93 % of the dataset, higher values dominated by Li, B, and Ga whilst the negative eigenvalues are predominantly Mg, Ca, Sn, and V. Concentrations of the higher PC4 values fit well to the geological boundaries of the SKD and CL (red, red-pink), whilst negative values appear more spread across the BVG, CM, WSG and SSG. Principal component 5 represents 5.02 % of the total data, positively contributed to by Co, U, Ni, and Mn in descending order of eigenvalue (Figure 5). These are notably concentrated within the Ennerdale and Eskdale granite boundaries, and clustered within the CL. Negative PC5 values are contributed to by Cu, Sr, Pb, Sn, and V which appear concentrated in the SKD. Dissimilar to PC1-3, the SKD and WSG are disaggregated by PC4 (red-pink) and PC5 (green). The WSG is now combined into PC5 along with parts of the northern section of CL. A mixture of PC4 and PC5 is shown in yellow, clustered within the Ennerdale granite and within the BVG where the felsic batholith below is at its topographic highest, indicating a potential felsic intrusive endmember chemistry. The Permian – Jurassic groups are not clearly defined, represented through a mix of PC4 and PC5 (purple-pink) which loosely follows the carbonates from the east and over the northern SKD and CM formation. Principal component 6 represents 4.55 % of the dataset. Higher PC6 values are dominated by Fe, Sr, Ca, V, and Mn whilst the negative eigenvalues are

predominantly Cu, B, and Pb. Concentrations of the higher PC6 values fit relatively within the geological boundaries of the BVG, with a clear boundary visible against the WSG (PC5), and across the CL and EVG (Figure 5).

Principal components 7 and 8 were analysed but don't clearly represent a distinct lithology and were therefore not included. For these component maps, and individual PC1-6 maps, refer to Appendix B.

4.2.2 K-means Cluster Analysis

A K-means cluster analysis was conducted on the calculated principal components. The optimal number of principal components to use was PC1-8, with the optimum number of clusters representing realistic geological linework being 7 (Figure 6); less than this and the geological boundaries appear to combine and any more creates illegible variation.

[Figure 6 here]

Cluster 1 had 713 data points, with 74.57 % of data within the geological boundaries of the WSG (Figure 6). This portion overlapped with 73.85 % of the WSG test data (Table 2) and outlined the WSG boundary clearly (Figure 6B). The remainder of cluster 1 was represented by 14 % CL (overlapping with 8% of CL test data), and low (< 5 %) CM, MFC, MMG, PS, SSG, and SKD. Although only 1.54 % of the total cluster 1 was MMG, it is important to note these overlapped with 75 % of the MMG test data.

[Table 2 here]

Cluster 2 had 226 data points, 73.01 % within the BVG. This only overlapped with 21.48 % of the total BVG test data which indicates a weak-moderate representation of this group by cluster 2 (Table 2). Of the remaining cluster 2, 19 % was OFPS (overlapping 41.35 % of OFPS test data), concentrated in the Ennerdale and NE Eskdale granites. The remainder was low

(<5 %) DMIS, SSG, and WSG. Only 1.33 % of cluster 2 was DPS, on the Shap granite (Figure 6C), but this overlapped with 42.85 % of DPS test data (Table 2).

Cluster 3 had 598 data points, split between the SKD (47.83 %) and the CL (39.13 %), with minor (<5 %) BVG, CM, EVG, OMIS, OMPS, MMG, MGG, LCTS, DPS, PS, SSG, and WSG. The SKD data in cluster 3 overlapped with 71.68 % of the SKD test data, distinguishing the main northern outcrop, the Black Combe inlier to the South, and two outcrops within the Eastern BVG (Figure 6D). The CL data overlapped with only 19.78 % of its test data (Table 2) restricted to the eastern outcrops. Although the contribution to this cluster by DPS was low, it overlapped with 71.68 % of the DPS test data (Table 2).

Cluster 4 had 467 data points, 80.09 % in the BVG which overlapped 48.7 % of BVG test data, clearly outlining the boundaries against the SKD, WSG and Eskdale / Ennerdale granties (Figure 6E). The OFPS contributed 6 %, and minor (<5 %) CL, EVG, DMIS, OMIS, MMG, DPS, SSG, SKD and WSG (Table 2). It is worth noting that despite a low proportion of OMPS, OMIS and DMIS, there is high overlap with their test data – 33.33 %, 50 %, and 33.33 % in the order stated.

Cluster 5 had 679 data points, split into 40.94 % CL, 27.25 % SSG, 8.39 % PS, 8.39 % MMG, and 5.74 % CM (Table 2). The remainder (<5 %) is BVG, OFPS, OMIS, MFC, MGG, LCTS, SKD, and WSG. The SSG data overlapped 57.28 % of SSG test data, the MMG overlapped with 50.89 % of test data, and the MGG overlapped 42.86 % of its test data, despite low proportional representation of these groups. Cluster 5 has sporadic data density creating poor geological resolution across all lithologies named (Figure 6F).

Cluster 6 had 684 data points, 63.16 % being CL overlapped with 36.52 % of CL test data (Figure 6G). The remainder is 9.06 % PS, 8.92 % SSG, 8.92 % CM, and minor (<5 %) BVG, EVG, OFPS, MMG, MGG, SKD, and LCTS (Table 2). Although there is low contribution from the PS and LCTS, these overlapped with 46.21 % and 50% of their respective test data. Similar to cluster 5 there is poor spatial resolution for geological boundaries.

Cluster 7 had 362 data points split between 31.49 % WSG, 27.62% BVG, 16.02 % CL, 12.98 % SKD, and 5.8 % EVG (Figure 6H). Minor contributors (<5 %) were the CM, DMIS, OFPS, OMPS, OMIS, MFC, LCTS, PS, and SSG (Table 2). It is worth noting that the EVG portion overlapped with 77.78 % of EVG test data. The low DMIS and OMPS overlapped with 33.33 % and 50 % of their respective test data. Spatial extent for this cluster is sporadic with the only geologically relevant concentrations within the EVG boundary.

4.3 Differentiation of Lithological Groups within Cluster Results

As this workflow uses large, multivariate elemental data it is expected that the K-means clustering will not yield perfect representations of a single lithological formation or group, especially when some are geochemically similar. To mitigate this, average chemistries of the real-world lithologies (test data) were used to manually disaggregate between any differing groups within the same cluster result, identifying key distinguishing element brackets.

The CL test data has higher Ca, Pb, Li and Zr averages and lower Cu, Mg, Ni, Sn and V compared to WSG test data (Figure 7A) and cluster 1 average (Figure 7B). Cluster 1 has lower As, Mn, Pb and Zn compared to WSG test data, the majority of elements except for Pb being in the same log-band. Data points with >200 ppm B, >250 ppm Zr, and >4000 ppm Ca were grouped into ‘CL + MFC associated’ data, isolating the WSG-associated points relatively successfully (Figure 7C). It is also possible to isolate CL-associated data from the MFC by identifying points < 12000 ppm Mg and >50 ppm Li (Figure 7C).

[Figure 7 here]

The BVG has higher Mg, Mn and Zn than the other data in cluster 2, with lower U. The OFPS-associated data were isolated by data >450 ppm Ba and >3 ppm U, separating the granite-associated data from the BVG / underlying batholith-associated data and from the Shap granite (DPS) (Figure 7C). Within cluster 3, CL test data are enriched in Ca and Zr and depleted in As, Be, Co, and Cu compared to the SKD test data and cluster 3 (Figure 7A, 7B).

The CL-associated data was isolated using <10 ppm Be, >250 ppm Zr and <6000 ppm Ti whilst SKD-associated data is <10 ppm Be, <250 ppm Zr, and >5000 ppm Ti (Figure 7C).

The remaining cluster results 4, 5, 6 and 7 were unable to be further disaggregated effectively into the known lithological groups.

4.4 Identification of Potential As-Co-Cu-Ni Mineralisation

As the SKD and BVG are the two main lithological groups associated with As-Co-Cu-Ni mineralisation, a more accurate understanding of their average ore-metal concentrations provides more specific insights into ore metal enrichment in the region.

4.4.1 Relative Enrichment of Ore Metals

The manually disaggregated SKD-associated data (see section 4.3) proved to be a moderately successful representation of the SKD test data ore metals (Figure 8). By removing the CL-associated data, the average value for these metals increased, most significantly for As, Co, Cu, Mo, and Zn. The data ranges for the SKD test data and disaggregated SKD Ag is very similar, with mean values of 0.27 ppm vs 0.33 ppm. The disaggregated SKD mean value for As (93.7 ppm), Co (63.26 ppm), and Zn (660.01 ppm) are significantly higher than the SKD test values, the As and Co being higher due to the removal of CL-associated data. All presented ore metal ranges overlapped with the test data ranges, with the mean values in the same logarithmic band (with exception to Mo and Zn, further indicating that the disaggregated values are a fair representation of the ‘true’ chemistries. All ore metal mean values in cluster 4 are in the same logarithmic range as the BVG test data (Figure 8) with very similar total ranges for each element, indicating cluster 4 is a fair representation of the BVG for these elements.

[Figure 8 here]

4.4.2 Modelled Lithogeochemistry Values vs Standard Baselines

Upon normalisation of the raw data G-BASE data to both the disaggregated SKD Co average (63.26 ppm), and cluster 4 Co average (26.86 ppm), there is a distinct reduction in Co anomalies across the SKD and BVG when compared to the empirical data alone, normalisation against average continental crust (CDT), and normalisation against upper continental crust (UCC) (Figure 9). This difference in baseline Co normalisation highlights relative anomalies between the two groups as the SKD had a higher average, making anomalies hosted here larger in ppm concentration than those in the BVG. The reduction in data points has removed 'noise' data, facilitating identification of higher and more accurate enrichments.

[Figure 9 here]

4.4.3 Prospective sites of As-Co-Cu-Ni Mineralisation

In order to assess the applicability of this geochemical workflow tool to mineral exploration, we combined the modelled average lithogeochemical data from the cluster results with other typical exploration criteria to identify As-Co-Cu-Ni prospective mineralisation.

Combined metal anomalies are useful for identifying this mineralisation style as typically there should be enrichment of all four elements, indicating co-mineralisation of As-, Cu-, Co-, Ni-bearing minerals. We identified anomalies here as concentrated clusters of data points with values >1 enrichment relative to the modelled SKD or BVG baselines for each of these elements. Figure 10 presents individual anomaly maps for As (Figure 10i), Co (Figure 10ii), Cu (Figure 10iii), and Ni (Figure 10iv) with a combined anomaly map to show where these elements all overlap (Figure 10A). Clusters of 'enriched' data points have been drawn around with polygons, the overlapping polygons then indicative of a combined anomaly. Further resolution is not possible with this data as stream sediment geochemistry is only indicative of the surrounding rock within the same drainage catchment, not the specific sampling site.

Catchments are important to exploration as they can geographically constrain the area surrounding anomalies, allowing more targeted exploration within these areas.

Below the SKD and BVG, outcropping as the Eskdale and Ennerdale granites, is a large batholith which has been long considered associated to Lake District mineralisation, and specifically As-Co-Cu-Ni-bearing veins (Ixer et al. 1979; Stanley 1982a; Solferino et al. 2021). The relative topography of this batholith to the surface is therefore an important aspect to consider, as the magmatic fluid and / or heat possibly had spatial control on the mineralisation at surface level. Therefore, shallower batholith topography was considered an indicator of more prospective sites. Regional and local scale faults are also associated with As-Co-Cu-Ni mineralisation (Solferino et al. 2021) as the faults act as a conduit for fluid migration, and possibly metal scavenging during transport (Millward et al. 1999). Lastly, historic mining sites were considered an exploration indicator as these can provide access to deeper rock units, spoil heap samples, and mineralisation from available samples or reports.

[Figure 10 here]

To quantify the prospectivity of areas of interest relative to these criteria, points have been assigned to each of the following factors:

- 1 point per overlapping element anomaly in the area (As, Co, Cu, Ni) – maximum 4 points.
- 2 points if anomalies are within a single drainage catchment, 1 point if spread across two catchments.
- 3 points if the anomalies are in proximity to batholith topography <1 km depth, 2 points if 1-3 km depth, and 1 point if 3-6 km depth.
- 3 points if the anomalies are in proximity to both regional and local scale faults (trending NESW), 2 points if just regional faults, 1 point if just local faults / different orientation trend.

- 1 point if anomalies are within the same drainage catchment as historic mining sites.

Using these, we identified 10 prospective areas of interest (Figure 10). The detailed breakdown of each site is summarised (Table 3) with the highest-ranking location being Crummock Water, Hartsop, and Hard Knott / Great How respectively. Notably, four of the prospective areas are proximal to known cobalt mineralisation: site 3 near Scar Crags (As-Co-Cu-Ni), site 4 near Dale Head north (As-Co-Cu), site 8 near Seathwaite (As-Co-Cu), and site 9 near Ulpha (As-Co-Cu).

[Table 3 here]

5 Discussion

5.1 Success of Geological Mapping Tools

The PCA was effective at differentiating the data into essentially rock-types and does reflect some of the smaller scale, nuanced geological features; however, for more robust classification of the rock-types into the established groups, the K-means clustering was essential.

To assess the overall success of the mapping tools, a combined approach is needed using:

1. High overlap % with test data = strong representation of true lithological formation or group..
2. High contribution of cluster % = strong representation of lithological formation or group by single cluster result.
3. Clear spatial coverage of known geological boundaries = strong representation of spatial extent of the geological contacts.

Without considering all three, results could be misleading e.g. high overlap with test data combined with high % contribution to a cluster could indicate success but be hiding poor data

coverage spatially across the lithological formation, an important aspect considering the use of this tool in geological mapping.

5.2 Identification of Ordovician - Silurian Sediments

5.2.1 Skiddaw Group (SKD)

The SKD is a ~5 km thick succession of greywackes and siltstones, outcropping dominantly in the Northern Fells region with more minor outcrops to the South (Black Combe inlier) and East (Ullswater, Bampton, Furness, Teesdale, and Cross Fell inliers) (Cooper & Molyneux. 1990; Johnson, 1961; Cooper et al, 1995). The SKD was well mapped by combined PC3 and PC4 represented by higher Ni, V, Cr, Mg, Li, B, Co, typical components to a shale lithology (Turekian & Wedepohl. 1961). There is a high overlap with SKD test data (71.68 %) by 47.83 % of cluster 3, meaning that the SKD is well represented by a single cluster result. The geological boundaries are distinct, isolating the northern SKD and Black Combe regions from the surrounding geology. To isolate the SKD completely from the CL in cluster 3, a supervised involvement was required to disaggregate the data using Be, Zr and Ti values. When using geochemical ranges, data to the western edge of the SKD is not retained, most likely due to crossing drainage basins with the neighbouring CL and CM, resulting in mixed geochemical signals. Despite this, the overall ability for geochemical mapping of the SKD is successful and involves mostly unsupervised methods.

5.2.2 Windermere Supergroup (WSG)

The WSG is shale-based lithologies but unlike the SKD, were deposited in a much deeper marine setting (Cameron et al. 1993). The WSG is clearly mapped by PC3 and PC5, the former indicating a strong Ni, V, Mg, Cr, Co signature similar to the SKD. Differentiating the two groups is PC6 with a strong Zn, U, Be, and Co signature. There is significantly high overlap with WSG test data (73.85 %) by 74.57 % of cluster 1, meaning that the WSG is represented well by this single cluster result. The geological boundary is clearly defined; therefore, the

WSG is successfully mapped completely unsupervised. Further disaggregation from sporadic data in the CL and MFC is possible using B, Ca, Mg, Li and Zr.

5.3 Identification of Devonian – Jurassic Sediments

5.3.1 Mell Fell Conglomerate (MFC)

The MFC is not clearly defined by the PCA, instead blending into the SKD (PC3) and BVG (PC2) surrounding it. There is overlap only by 1.26 % of cluster 1 onto 75 % of the MFC test data. Spatially the geological boundaries are defined moderately well, although not absolutely clear. It is possible to disaggregate the MFC data from the WSG data in cluster 1 using B, Zr and Ca but it is not possible to ungroup it from the CL-associated data. The overall mapping success of the MFC is therefore moderately unsuccessful.

5.3.2 Carboniferous Limestone (CL)

Through a combination of PC1 and PC3, the CL is outlined relatively clearly although there is mixing with sandstones also defined by PC1. The clearest geological boundaries are defined to the East and North, where sample density is more concentrated. A combination of clusters 3, 5 and 6 is necessary to accommodate all data points assigned to the CL test data: 39.13 % of cluster 3 overlapping 19.78 % of CL test data with poor boundary resolution; 40.94 % of cluster 5 overlapping 23.5 % of CL test data with moderately poor boundary resolution; 63.16 % of cluster 6 overlapping 36.52 % of CL test data, with stronger boundary resolution. A supervised approach is necessary to disaggregate the CL data from others in the same cluster e.g., in cluster 3 separating CL from the SKD using Be, Zr and Ti. Although there is a significant outcrop presence of this group, low-density sampling results in poor-moderate mapping success.

5.3.3 Millstone Grit Group (MGG)

The MGG has relatively little outcrop at surface and is indistinguishable using a PCA, the only part notable being the largest outcrop to the South-East, within the CL, shared between PC1-2. The majority of MGG data is shared between clusters 3, 5 and 6 with little clarity on geological boundaries. It is worth noting that 21.43 % of the MGG test data was unconsidered during the K-means clustering analysis. Furthermore, inability to manually distinguish the MGG using geochemical ranges consigns the mapping success to very poor.

5.3.4 Coal Measures (CM)

Using a PCA, the CM blended with the neighbouring lithologies within PC1 and PC3. The CM is split between clusters 3, 5 and 6 with strongest overlap of test data through cluster 6 (46.21 % overlapped). Geological boundaries are poorly constrained, especially in the West, with low density of points within the CM boundaries. This combined with the inability to geochemically disaggregate the data results in poor mapping success.

5.3.5 Permian Sandstone, Mudstone and Conglomerate (PS)

Within PC1, the PS merges with the CL directly west, and with the CM and SSG to the north. There is however still some definition against the SKD, BVG, and WSG. The data points for this group are split between 8.93 % of cluster 5, and 9.06 % of cluster 6, overlapping with 42.54 % of test data for cluster 5, and 46.27 % of cluster 6, a pretty even division. The PS are also difficult to distinguish manually using geochemistry. Therefore, a combination of poor geological resolution, the need for multiple clusters to represent the group, and lack of bracketable geochemical signatures results in poor mapping success.

5.3.6 Sherwood Sandstone Group (SSG)

Through a combination of PC1 (dominantly) and PC2, the eastern outcrops of the SSG represent the geological boundaries well, although the northern outcrop between the MMG and CM is less so. 57.28 % of the SSG test data overlapped by 27.5 % of cluster 5, and 18.89

% of the test data by 8.92 % of cluster 6 –indicating a shared representation. Cluster 5 has the most data from the SSG and there are clusters of points following the boundaries of the SSG eastern outcrop, but less so in the north and in cluster 6. This poor resolution combined with the inability for geochemical disaggregation results in only moderately successful mapping.

5.3.7 Mercia Mudstone Group (MMG)

The MMG blended into PC1-3 with the CL, CM and SSG. This group did have better resolution in PC5-6 (PC6 dominating in light blue), partially outlining the geological boundaries. 8.39 % of cluster 5 overlaps with 50.89 % of MMG test data, and 2.92 % of cluster 6 with 17.86% test data. The overall mapping success was relatively moderate.

5.4 Identification of Ordovician Volcanics (BVG, EVG)

Forming contemporaneously with the upper SKD was the EVG basaltic-rhyolitic lavas (Moseley, 1978; Toghill, 2000). Then came the BVG marking a distinct change in depositional setting to subaerial calc-alkaline volcanism (Cameron et al. 1993) during the same subduction period as the EVG. The EVG was not clearly defined by the PCA, whilst the BVG was distinctly defined by PC2, isolating the calc-alkaline volcanics from the neighbouring shales and granites with a strong Rb, Ga, V, Be, and Al signature. Principal component 6 also defined the BVG, creating more colour fluctuation, possibly representing local geological variation between the BVG and underlying batholith signature.

The majority (77.78 %) of EVG test data was overlapped by 5.8 % of cluster 7 with strong concentration of data points within the boundaries. The EVG cannot be distinguished any further using manual geochemical ranges, therefore has moderate mapping success. On the other hand, the BVG was clearly defined by cluster 4 with 80.09 % of the cluster overlapped by 48.7 % of the BVG test data, with defined geological boundaries. The BVG was successfully mapped completely unsupervised, with clear boundaries against the SKD, WSG and OFPS.

5.5 Identification of Ordovician Igneous Lithology (OMIS, OMPS, OFPS)

The OMIS and OMPS are unclear on the combined PCA maps, most likely due to the relatively small outcrop extent. Cluster analysis grouped these mostly into clusters 3, 4 and 7 but due to the low number of data points assigned to the test data, an implication of low-spatial extent for the spatial-joining process (see Methods), there was no clear definition of these groups. These intrusions are relatively small-scale and are spread across the SKD and BVG, therefore the geochemical signatures were being masked by the dominant sediment / volcanic signatures and cannot be represented by the G-BASE data.

The much larger outcropping Eskdale and Ennerdale granites, representing the OFPS, were able to be mapped using this workflow. The Ennerdale granite is well outlined by a combination of PC4-5 (yellow) although the Eskdale is not, most likely due to overlapping drainage basins with the neighbouring BVG, resulting in the blue volcanic signature of PC6 to overlay the Eskdale geological boundary. The same was noted by cluster 2, with concentrations strongly in the Ennerdale but weakly in the Eskdale. These are better defined using Ba and U to manually disaggregate the data. Improved mapping of the Eskdale granite could be possible using other techniques such as combining gravity anomaly data into the PCA (Wang et al. 2011) or using U in regression modelling (Parsa et al. 2016); however, the success of this specific workflow is sufficient.

5.6 Identification of Devonian - Carboniferous Igneous Groups (DPS, DMIS, LCTS)

The smaller DMIS and LCTS were not clearly identified using the PCA. Clusters 1, 4 and 7 split the data associated with the DMIS, whilst cluster 6 represented the data for the LCTS, albeit both with poor geological resolution. This poor mapping was due to the low number of data points within the test data, a similar issue faced by the Ordovician igneous groups.

The DPS, most represented at the surface as the Shap granite outcrop, was clearly defined using a PCA, noted in PC2 (green) blended with other volcanics, and PC4 (red) blended with the SKD, possibly though shared strong element signatures like Li. The majority of DPS was represented by clusters 2 and 3, with cluster 2 concentrating in Shap and the cluster 3 data most likely blended between the SKD and minor DPS outcrops within the SKD boundary. The mapping of the DPS is therefore partially successful, requiring the combination of two cluster results or two principal components.

5.7 Limitations to Geological Mapping Tool

5.7.1 Mapping Capabilities

The first key limitation to this workflow is that stream sediment data can only represent lithogeochemistry to a certain level of success as a variety of factors can influence the measured chemical signatures: e.g., mixing of rock types in source drainage basin, weathering, soil, anthropogenic contamination, poor sampling practises, and poor sample preparation practises etc. These need to be considered when conducting geochemical mapping, especially in the Lake District where mining spoil heaps are known to influence soil and groundwater chemistries (Potter et al. 2004; Schillereff et al. 2016), and mountainous topography creates smaller, more constrained drainage basins. Topographic control on data collection (i.e., more mountainous areas create smaller, sharper watersheds which combined with higher resolution sampling leads to more defined geological boundaries) affects the overall mapping capabilities. The relative success of this method in more flat-terrain regions with more sporadic sampling would be lower, obvious when we consider the successful results of the SKD, BVG, and WSG here in mountainous, higher sample density areas which leads to better mapping success, compared to the poorer success of Carboniferous - Jurassic sediments in more flat terrain with sparse sampling.

The rock types mapped in this study are mostly sedimentary-volcanic based with minor felsic and mafic intrusive bodies. This study did not include significantly metamorphosed or ultramafic lithologies, excluding the metamorphic Crummock Aureole which forms part of the western SKD: depleted in Cu, Fe, Li, and Mn but enriched in Ca, F, Si, Co and Pb (Cooper et al. 1988; Fortey NJ. 1989). The capability of the G-BASE data to map highly metamorphosed and ultramafic rock types successfully therefore requires further investigation as this should be entirely possible (Cocker MD. 1999; Ranasinghe et al. 2009; Yilmaz et al. 2015; Vicente et al. 2021).

5.7.2 Data Availability

Geochemical investigations using stream sediment data requires access to large, multivariate geochemical datasets, especially when looking at regional scale. This is possible for well investigated countries such as the UK, USA, Europe, and Asia where regional mapping surveys have been completed (Xuejing et al. 1997; Johnson et al. 2005; Ohta et al. 2005; Xuejing et al. 2008; Salminen et al. 2012; Smith et al. 2013) and digital repositories are available; however, data may be much harder to access in other areas of the world where mineral exploration occurs.

5.7.3 Supervised Involvement in Workflow

Manual disaggregation of the K-means cluster results was possible to isolate specific groups within the same cluster, for example in this study in clusters 1, 2 and 3. This does require prior knowledge of expectant geological formations and geochemistry to assess mapping success, somewhat removing the autonomy of the workflow and applicability to regions with lesser-known geology. Similarly, low data point density and excessively overlapped geochemistries led to the inability to disaggregate formations and groups within clusters 4-7. With further experimentation it could be possible to identify element brackets to disaggregate clusters in other areas; however, this requires a lot of manual input to determine how successful this could be in a scenario without having test data for comparison.

5.8 Prospective As-Co-Cu-Ni Mineralisation

Epigenetic mineralisation occurred almost exclusively throughout the SKD, EVG, and BVG. Identifying As-Co-Cu-Ni mineralisation here has real-world applicability to prospective mineral identification elsewhere in similar settings (i.e., sedimentary-volcanic terrains, proximity to shallow batholith bodies and igneous-associated regional structures etc.).

Although mineral exploration into the Lake District is not a novel study (Mallick DIJ 1981; Shepherd & Waters. 1984; Cameron et al. 1993), the combination of literature-based information, geospatial data, and modelled ore metal chemistries from this study have identified 10 prospective areas for further investigation. This is specifically for As-Co-Cu-Ni mineralisation, other local mineralisation styles falling outside of the remit of this study (e.g. Baryte-Pb-Zn). This being said, there is no reason why this workflow could not be used for these other mineralisation styles, further investigation of this should be strongly encouraged and tested. The advantage to using stream sediment geochemistry is the access of the river sediments to deeper lithology not visible at the surface, including veins which are typically covered by vegetation or the more sulphide-rich phases not at an observable level relative to modern topography (typically forming at mid-shallow crustal depths in geological time). The overlap of 4 of these 10 prospective areas with known Co mineralisation: Scar Crags, Dale Head North, Ulpha and Seathwaite (Stanley & Criddle, 1979; Ixer et al 1979; Stanley & Vaughan 1982a; Solferino et al 2021; Eskdale et al. 2021), indicates that this workflow was relatively successful, although in-field verification is required at the other 6 sites before the true success can be determined. This will involve local sampling of host rocks and visible mineralisation, smaller scale drainage basin mapping, and further geochemical analysis to confirm Co concentrations and vein-based ore metal assemblages.

5.9 Applicability of Workflow for Future Geological Mapping and Exploration Projects

From the successes of this study, we would recommend that the following workflow be followed for repetition of this combined unsupervised-supervised analytical approach, especially when using similar scale geochemical datasets and in areas where a geochemical / geological map would benefit the exploration study.

Stream sediment geochemical data should ideally be collected in a high-resolution sampling campaign, with more concentrated sampling across lower-topographic areas to ensure mapping resolution is maintained comparatively to mountainous areas. Once all QAQC procedures are complete and raw data is available for use, a PCA followed by a K-means clustering analysis should be conducted. It is essential prior to the PCA to conduct a CLR transformation on the data in order to follow CoDA standards for geochemical compositional data (Buccianti A. 2011; Wang et al. 2014; Buccianti & Grunsky. 2014). This is all conductible through the use of ioGAS.64 and QGIS software, although various R packages (‘compositions’, ‘robComposition’) exist which also work well with compositional data and can be an open-source alternative to ioGAS statistics (Templ et al. 2011; Gerald van den Boogaart et al. 2022). Finally, it is advised to create geochemical ranges within the cluster results in an attempt to identify any possibility for further disaggregation of lithological groups. The results should then be compared to any known data for evaluation of success (i.e., existing geological maps for the area), followed by in-field verification. For visualisation of this study’s workflow refer to Appendix D.

6 Conclusions

Using a combination of PCA, K-means clustering, and available exploration-related data (geological maps, geophysical surveys, structural and mining maps) it is possible to determine

several factors regarding the success of using G-BASE stream sediment data as a geological mapping tool, and mineral exploration tool for As-Co-Cu-Ni anomalies in Cumbria.

This workflow has geochemically mapped the sedimentary-volcanic lithological groups across Cumbria at a 50k resolution, with successful results. This includes known ore-bearing lithologies in the region, such as the SKD and BVG, and large igneous bodies including the Eskdale, Ennerdale and Shap granites. The success of this mapping workflow has been identified to rely on several parameters: (a) sufficient geochemical sampling resolution (=<1 km); (b) topographic suitability; (c) extent of geological outcrop at surface level. If these criteria are met then this workflow can be applied, rapidly and reliably providing insight into both geology and geochemistry at scale.

Average geochemistries have been defined for the SKD and BVG groups, providing higher resolution and more accurate As-Co-Cu-Ni anomaly maps by using these results as baselines for enrichment. Although geological mapping using the G-BASE dataset has been practised elsewhere (e.g. Kirkwood et al. 2016b; BGS 1992), the use of this data in conjunction with mineral exploration for As-Co-Cu-Ni mineralisation has not yet been attempted and has yielded interesting results. We identified 10 prospective areas of interest for As-Co-Cu-Ni mineralisation, four of which lie in close proximity (same / neighbouring drainage basin) to pre-identified As-Co-Cu-Ni mineralisation. There is a serious possibility the other 6 sites may identify previously unknown mineralisation of the same style, therefore in-field verification is needed to establish this.

Finally, it is worth noting that this workflow is critically applicable to exploration due to the relatively little time involved post-sampling. Complex and diverse geochemical analysis is shown to be conducted on raw data within a very short timeframe. Although problematic issues using this method need to be acknowledged (e.g. stream sediment geochemistry not being fully representative of host rock, poor data density etc.), the processing time from raw multivariate element data, to inputting into ioGAS / QGIS, and receiving spatially relevant results is minutes to hours. This has obvious practical applications within the explorative

industry, but also any company / initiative that needs quantitative, geochemical investigations into previously uncertain geological terrains. For example, areas where geological maps were constructed almost half a century ago can now be tested for robustness in a matter of hours with very little effort by the research team as long as the required data has is available, which for areas like Europe, US and Asia is perfectly feasible with modern sampling campaigns and open-access data repositories available online. This does of course rely on similar explorative geochemical projects like G-BASE and TELLUS to be conducted in the areas of interest; however, with multiple stakeholders interested in prospective regions this could possibly be compiled from existing legacy data or through future collaborative effort. The principal idea that someone can never have had physical presence in an area but be able to define lithological boundaries, highlight potential ore enrichment combined with known metallogenetic factors (chemical associations, rock types, structures), and apply this to their exploration campaign with statistical robustness is a key tool. Although this thought process towards geochemical data is already well-practised, the ability to conduct such work at a fully remote, low-cost level is worth highlighting.

7 Acknowledgements

The authors would like to thank the BGS for providing access to the G-BASE data used in this study, data derived from 1:50,000 scale BGS Digital Data under Licence No. 2021/026 British Geological Survey © UKRI. All rights reserved. AE was supported in this research by the Royal Holloway University of London, Department of Earth Sciences Reid Scholarship. We thank the Department of Earth Sciences Research Committee at Royal Holloway, University of London, for providing financial assistance for conference and networking that assisted in the construction of this manuscript.

8 Conflict of Interest

The authors declare that there are no conflicts of interest in relation to this research.

9 References

Aitchison, J., 1982, The Statistical Analysis of Compositional Data: Journal of the Royal Statistical Society: Series B (Methodological), v. 44, p. 139–160, doi:https://doi.org/10.1111/j.2517-6161.1982.tb01195.x.

Alves, P.D., Pavel, C., Blagoeva, D., and Arvanitidis, N., 2018, Cobalt: demand-supply balances in the transition to electric mobility.

van den Boogaart, K., and Tolosana-Delgado, R., 2008, “Compositions”: a unified R package to analyze compositional data, p. 320–338.

Bott, M.H.P., 1974, The geological interpretation of a gravity survey of the english lake District and the Vale of Eden: Journal of the Geological Society, v. 130, p. 309–331, doi:10.1144/gsjgs.130.4.0309.

Branney, M.J., and Soper, N.J., 1988, Ordovician volcano-tectonics in the English Lake District.: Journal - Geological Society (London), v. 145, p. 367–376, doi:10.1144/gsjgs.145.3.0367.

Brown, G., 1980, Lake District Sheet 54N - 04W, 1:250 000 Series Solid Geology: , p. 1.

Buccianti, A., 2011, Natural Laws Governing the Distribution of the Elements in Geochemistry: The Role of the Log-Ratio Approach: Compositional Data Analysis: Theory and Applications, p. 255–266, doi:10.1002/9781119976462.CH18.

Buccianti, A., and Grunsky, E., 2014, Compositional data analysis in geochemistry: Are we sure to see what really occurs during natural processes? Journal of Geochemical Exploration, v. 141, p. 1–5, doi:10.1016/J.GEXPLO.2014.03.022.

Cameron, D.G., Cooper, D., Johnson, E., Roberts, P., Cornwall, J., Bland, D., and Nancarrow, P., 1993, Mineral exploration in the Lower Palaeozoic rocks of south–west Cumbria. Part 1: Regional Surveys.

Capewell, J.G., 1955, The Post-Silurian Pre-Marine Carboniferous Sedimentary Rocks of the Eastern Side of the English Lake District: Quarterly Journal of the Geological Society, v. 111, p. 23–46, doi:10.1144/GSL.JGS.1955.111.01-04.03.

Chenery, S., Ander, E., Perkins, K., and Smith, B., 2002, Uranium anomalies identified using G-BASE data - Natural or anthropogenic ? A uranium isotope pilot study.

Cocker, M.D., 1999, Geochemical mapping in Georgia, USA: a tool for environmental studies, geologic mapping and mineral exploration: Journal of Geochemical Exploration, v. 67, p. 345–360, doi:https://doi.org/10.1016/S0375-6742(99)00079-5.

Cooper, D.C., Lee,', M.K., Fortey, N.J., Cooper, A.H., Rundle, C.C., Webb2, B.C., and Allen, P.M., 1988, The Crummock Water aureole: a zone of metasomatism and source of ore metals in the English Lake District.

Cooper, A.H., and Molyneux, S.G., 1990, The age and correlation of Skiddaw Group (early Ordovician) sediments in the Cross Fell inlier (northern England): Geological Magazine, v. 127, p. 147–157, doi:10.1017/S0016756800013832.

Cooper, A.H., Rushton, A.W.A., Molyneux, S.G., Hughes, R.. A., Moore, R.M., and Webb, B.C., 1995, The stratigraphy, correlation, provenance and palaeogeography of the Skiddaw Group (Ordovician) in the English Lake District: Geological Magazine, v. 132, p. 185–211.

Dagger, G.W., 1977, Controls of copper mineralization at Coniston, English Lake District: Geological Magazine, v. 114, p. 195–202, doi:10.1017/S0016756800044769.

Darton Commodities, 2020, Cobalt Market Review 2019-2020.

Dehaine, Q., Michaux, S.P., Butcher, A.R., and Cook, N., 2021, Geometallurgical characterisation of the Rajapalot Au-Co project - BATCircle Project Report 04

Eskdale, A.E., Gough, A., Lowry, D., and Johnson, S.C., 2021, Metallogenesis of Cobalt-bearing Mineralisation in the English Lake District. doi:10.7185/gold2021.3717.

Everett, P.A., Lister, T.R., Fordyce, F.M., Ferreira, A.M.P.J., Donald, A.W., Gowing, C.J.B., and Lawley, R.S., 2019, Stream sediment geochemical atlas of the United Kingdom: 1–94 p.

Firman, R., 1978, Epigenetic Mineralisation, in The Geology of the Lake District, p. 226–241.

Firman, R., and Lee, M.K., 1986, Age and structure of the concealed English Lake District hatholith and its probable influence on subsequent sedimentation, tectonics and mineralization.: Geology in the Real World - the Kingsley Dunham volume, p. 117–127.

Fortey, N.J., 1989, Low grade metamorphism in the Lower Ordovician Skiddaw Group of the Lake District, England: Proceedings of the Yorkshire Geological Society, v. 47, p. 325–337, doi:10.1144/pygs.47.4.325.

Gallagher, V., Grunsky, E.C., Fitzsimons, M.M., Browne, M.A., Lilburn, S., and Symons, J., 2022, Tellus regional stream water geochemistry: environmental and mineral exploration applications: Geochemistry: Exploration, Environment, Analysis, v. 22, p. geochem2021-050, doi:10.1144/geochem2021-050.

Gazley, M.F., Collins, K.S.S., Hines, B.R.R., Fisher, L.A.A., and McFarlane, A., 2015, Application of principal component analysis and cluster analysis to mineral exploration and mine geology and cluster analysis to mineral exploration, in AusIMM New Zealand Branch Annual Conference 2015, p. 131–139.

Grunsky, E.C., 2010, The interpretation of geochemical survey data: Geochemistry: Exploration, Environment, Analysis, v. 10, p. 27–74, doi:10.1144/1467-7873/09-210.

Grunsky, E.C., and de Caritat, P., 2020, State-of-the-art analysis of geochemical data for mineral exploration: Geochemistry: Exploration, Environment, Analysis, v. 20, p. 217–232, doi:10.1144/geochem2019-031.

Gulley, A.L., 2022, One hundred years of cobalt production in the Democratic Republic of the Congo: Resources Policy, v. 79, p. 103007,

doi:https://doi.org/10.1016/j.resourpol.2022.103007.

Hitzman, M.W., Bookstrom, A.A., Slack, J.F., and Zientek, M.L., 2017, Cobalt—Styles of Deposits and the Search for Primary Deposits: USGS Open-File Report, v. 0, p. 53, doi:10.3133/ofr20171155.

Hughes, R.A., Evans, J.A., Noble, S.R., and Rundle, C.C., 1996, U-Pb chronology of the Ennerdale and Eskdale intrusions supports sub-volcanic relationships with the Borrowdale Volcanic Group (Ordovician, English Lake District): Journal of the Geological Society, v. 153, p. 33–38, doi:10.1144/gsjgs.153.1.0033.

Hund, K., La Porta, D., Fabregas, T., Laing, T., and Drexhage, J., 2020, Minerals for Climate Action: The Mineral Intensity of the Clean Energy Transition: World Bank Publications, p. 110.

Ixer, R.A., Stanley, C.J., and Vaughan, D.J., 1979, Cobalt-, nickel-, and iron-bearing sulpharsenides from the north of England: Mineralogical Magazine, v. 43, p. 389–395, doi:10.1180/minmag.1979.043.327.11.

Johnson, G., 1961, Skiddaw Slates proved in the Teesdale Inlier: Nature, v. 190, p. 996–997, doi:10.1038/190996a0.

Johnson, C.C., Breward, N., Ander, E.L., and Ault, L., 2005, G-BASE: Baseline geochemical mapping of Great Britain and Northern Ireland: Geochemistry: Exploration, Environment, Analysis, v. 5, p. 347–357, doi:10.1144/1467-7873/05-070.

Johnson, C.C., Cave, M., Napier, A., and Mackenzie, A.C., 2011, Displaying G-BASE geochemical sample information in Google Earth.

Kaiser, H.F., 1960, The Application of Electronic Computers to Factor Analysis: Educational and Psychological Measurement, v. 20, p. 141–151, doi:10.1177/001316446002000116.

Kirkwood, C., Cave, M., Beamish, D., Grebby, S., and Ferreira, A., 2016a, A machine learning approach to geochemical mapping: Journal of Geochemical Exploration, v. 167, p. 49–

61, doi:10.1016/j.gexplo.2016.05.003.

Kirkwood, C., Everett, P., Ferreira, A., and Lister, B., 2016b, Stream sediment geochemistry as a tool for enhancing geological understanding: An overview of new data from south west England: Journal of Geochemical Exploration, v. 163, p. 28–40, doi:10.1016/j.gexplo.2016.01.010.

Kissin, S.A., 1992, Five-element (Ni-Co-As-Ag-Bi) veins: Geoscience Canada, v. 19, p. 113–124.

Lapworth, D.J. et al., 2012, Geochemical mapping using stream sediments in west-central Nigeria: Implications for environmental studies and mineral exploration in West Africa: Applied Geochemistry, v. 27, p. 1035–1052, doi:https://doi.org/10.1016/j.apgeochem.2012.02.023.

Lawie, D., 2010, EXPLORATORY DATA ANALYSIS FOR TARGET Altered basalts: , p. 77–80.

Lister, T.R., and Johnson, C.C., 2005, G-BASE data conditioning procedures for stream sediment and soil geochemical analyses.

Lott, G., and Parry, S., 2017, Strategic Stone Study - A Building Stone Atlas of Cumbria and The Lake District.

Mallick, D.I.J., 1981, I.G.C.P. project no. 143—Remote sensing and mineral exploration: Current UK activities: Advances in Space Research, v. 1, p. 285–288, doi:10.1016/0273-1177(81)90405-1.

Millward, D., Beddoe-Stephens, B., and Young, B., 1999, Pre-acadian copper mineralization in the English Lake District: Geological Magazine, v. 136, p. 159–176, doi:10.1017/S0016756899002289.

Millward, D., Beddoe-Stephens, B., and Young, B., 1978, The Eycott and Borrowdale volcanic rocks., in The Geology of the Lake District, p. 99–120.

Moseley, F., 1978, The Geology of the Lake District: Yorkshire Geological Society, 284 p.

Nguyen, R.T., Eggert, R.G., Severson, M.H., and Anderson, C.G., 2021, Global Electrification of Vehicles and Intertwined Material Supply Chains of Cobalt, Copper and Nickel: Resources, Conservation and Recycling, v. 167, p. 105198, doi:https://doi.org/10.1016/j.resconrec.2020.105198.

O'Brien, C., Plant, J.A., Simpson, P.R., and Tarney, J., 1985, The geochemistry, metasomatism and petrogenesis of the granites of the English Lake District: Journal of the Geological Society, v. 142, p. 1139–1157, doi:10.1144/gsjgs.142.6.1139.

Ohta, A., Imai, N., Terashima, S., and Tachibana, Y., 2005, Application of multi-element statistical analysis for regional geochemical mapping in Central Japan: Applied Geochemistry, v. 20, p. 1017–1037. doi:https://doi.org/10.1016/j.apgeochem.2004.12.005.

Parsa, M., Maghsoudi, A., and Ghezelbash, R., 2016, Decomposition of anomaly patterns of multi-element geochemical signatures in Ahar area, NW Iran: a comparison of U-spatial statistics and fractal models: Arabian Journal of Geosciences, v. 9, p. 260, doi:10.1007/s12517-016-2435-5.

Pharaoh, T.C., 1999, Palaeozoic terranes and their lithospheric boundaries within the Trans-European Suture Zone (TESZ): A review: Tectonophysics, v. 314, p. 17–41, doi:10.1016/S0040-1951(99)00235-8.

Potter, H., Bone, B., Forster, J., Chatfield, P., and Tate, G., 2004, The Environment Agency's approach to mining pollution: Proc IMWA Symp: Mine Water.

Ranasinghe, P.N., Fernando, G.W.A.., Dissanayake, C.B., Rupasinghe, M.S., and Witter, D.L., 2009, Statistical evaluation of stream sediment geochemistry in interpreting the river catchment of high-grade metamorphic terrains: Journal of Geochemical Exploration, v. 103, p. 97–114, doi:https://doi.org/10.1016/j.gexplo.2009.07.003.

Rawlins, B., McGrath, S., Scheib, A., Breward, N., Cave, M., Lister, T.R., Ingham, M., Gowing, C., and Carter, S., 2012, The advanced soil geochemical atlas of England and Wales.

Regional Geochemistry of the Lake District and adjacent areas., 1992, Nottingham.

Russell, A., 1925, A notice of the occurrence of native arsenic in Cornwall ; of bismuthinite at Shap, Westmorland ; and of smaltite and niccolite at Coniston, Lancashire: Mineralogical Magazine and Journal of the Mineralogical Society, v. 20, p. 299–304, doi:10.1180/minmag.1925.020.108.05.

Salminen, R. et al., 1998, FOREGS Geochemical Mapping Field Manual.

Salomão, G.N. et al., 2020, Geochemical mapping in stream sediments of the Carajás Mineral Province: Background values for the Itacaiúnas River watershed, Brazil: Applied Geochemistry, v. 118, p. 104608, doi:https://doi.org/10.1016/j.apgeochem.2020.104608.

Scheib, A.J., Breward, N., Lawley, R., Johnson, C., Nice, S., and Lee, J., 2007, Investigation of G-BASE regional soil geochemistry over Pleistocene till deposits in East Anglia using factor analysis.

Schillereff, D.N., Chiverrell, R.C., Macdonald, N., Hooke, J.M., and Welsh, K.E., 2016, Quantifying system disturbance and recovery from historical mining-derived metal contamination at Brotherswater, northwest England: Journal of Paleolimnology, v. 56, p. 205–221, doi:10.1007/s10933-016-9907-1.

Scoon, R.N., 2021, The Lake District, Northwest England, in the Geotraveller, Springer, doi:https://doi.org/10.1007/978-3-030-54693-9_16.

Shepherd, T.J., and Waters, P., 1984, Fluid inclusion gas studies, carrock fell tungsten deposit, england: implications for regional exploration: Mineralium Deposita 1984 19:4, v. 19, p. 304–314, doi:10.1007/BF00204385.

Smith, D.B., Smith, S.M., and Horton, J.D., 2013, History and evaluation of national-scale geochemical data sets for the United States: Geoscience Frontiers, v. 4, p. 167–183,

doi:https://doi.org/10.1016/j.gsf.2012.07.002.

Solferino, G.F.D., Westwood, N.T., Eskdale, A., and Johnson, S.C., 2021, Characterising As–Bi–Co–Cu-bearing minerals at Scar Crags and Dale Head North, Lake District, UK: Mineralogical Magazine, v. 85, p. 197–214, doi:10.1180/mgm.2021.22.

Stanley, C.J., and Criddle, A.J., 1979, Mineralization at Seathwaite Tarn, near Coniston, English Lake District: The first occurrence of wittichenite in Great Britain: Mineralogical Magazine, v. 43, p. 103–107.

Stanley, C.J., and Vaughan, D.J., 1982a, Copper, lead, zinc and cobalt mineralization in the English Lake District: classification, conditions of formation and genesis.: Journal of the Geological Society, v. 139, p. 569–579, doi:10.1144/gsjgs.139.5.0569.

Stanley, C.J., and Vaughan, D.J., 1980, Interpretative Studies of Copper Mineralization To the South of Keswick, England.: Transactions of the Institution of Mining and Metallurgy, Section B: Applied Earth Science, v. 89.

Stanley, C.J., and Vaughan, D.J., 1982b, Mineralization in the Bonser vein, Coniston, English Lake District: mineral assemblages, paragenesis, and formation conditions: Mineralogical Magazine, v. 46, p. 343–350, doi:10.1180/minmag.1982.046.340.08.

Steiner, B., 2018, Using Tellus stream sediment geochemistry to fingerprint regional geology and mineralisation systems in Southeast Ireland: Irish Journal of Earth Sciences, v. 36, p. 45–61.

Stephenson, D., Bevins, R.E., Millward, D., Highton, A.J., Parsons, I., Stone, P., and Wadsworth, W.J., 1999, Caledonian Igneous Rocks of Great Britain: Geological Conservation Review Series, p. 648.

Stone, P., Millward, D., Young, B., Merritt, J., Clarke, S., McCormac, M., and Lawrence, D., 2010, British regional geology: Northern England.: Nottingham, British Geological Survey.

Tabelin, C.B., Park, I., Phengsaart, T., Jeon, S., Villacorte-Tabelin, M., Alonzo, D., Yoo, K., Ito, M., and Hiroyoshi, N., 2021, Copper and critical metals production from porphyry ores and E-wastes: A review of resource availability, processing/recycling challenges, socio-environmental aspects, and sustainability issues: Resources, Conservation and Recycling, v. 170, p. 105610, doi:https://doi.org/10.1016/j.resconrec.2021.105610.

Tait, J.A., Bachtadse, V., Franke, W., and Soffel, H.C., 1997a, Geodynamic evolution of the European Variscan fold belt: palaeomagnetic and geological constraints: Geologische Rundschau, v. 86, p. 585–598, doi:10.1007/s005310050165.

Tait, J.A., Bachtadse, V., Franke, W., and Soffel, H.C., 1997b, Geodynamic evolution of the European Variscan fold belt: Palaeomagnetic and geological constraints: International Journal of Earth Sciences, v. 86, p. 585–598.

Toghill, P., 2000, The Geology of Britain: An Introduction: Marlborough, The Crowood Press Ltd, 224 p.

Torsvik, T.H., Smethurst, M.A., Meert, J.G., Van Der Voo, R., McKerrow, W.S., Brasier, M.D., Sturt, B.A., and Walderhaug, H.J., 1996, Continental break-up and collision in the Neoproterozoic and Palaeozoic - A tale of Baltica and Laurentia: Earth-Science Reviews, v. 40, p. 229–258, doi:10.1016/0012-8252(96)00008-6.

Turekian, K., and Wedepohl, K., 1961, Distribution of the Elements in Some Major Units of the Earth's Crust: GSA Bulletin, v. 72, p. 175–192, doi:10.1130/0016-7606(1961)72[175:DOTEIS]2.0.CO;2.

Vicente, V.A.S., Pratas, J.A.M.S., Santos, F.C.M., Silva, M.M.V.G., Favas, P.J.C., and Conde, L.E.N., 2021, Geochemical anomalies from a survey of stream sediments in the Maquelab area (Oecusse, Timor-Leste) and their bearing on the identification of mafic-ultramafic chromite rich complex: Applied Geochemistry, v. 126, p. 104868, doi:https://doi.org/10.1016/j.apgeochem.2020.104868.

Walton, A. et al., 2021, Securing technology-critical metals for Britain: University of Birmingham.

Wang, W., Zhao, J., and Cheng, Q., 2011, Analysis and integration of geo-information to identify granitic intrusions as exploration targets in southeastern Yunnan District, China: Computers & Geosciences, v. 37, p. 1946–1957, doi:https://doi.org/10.1016/j.cageo.2011.06.023.

Wang, W., Zhao, J., and Cheng, Q., 2014, Mapping of Fe mineralization-associated geochemical signatures using logratio transformed stream sediment geochemical data in eastern Tianshan, China: Journal of Geochemical Exploration, v. 141, p. 6–14, doi:10.1016/j.gexplo.2013.11.008.

Woodcock, N.H., Soper, N.J., and Miles, A.J., 2019, Age of the Acadian deformation and Devonian granites in northern England: a review:, doi:10.1144/pygs2018-009.

Xie, X., Wang, X., Zhang, Q., Zhou, G., Cheng, H., Liu, D., Cheng, Z., and Xu, S., 2008, Multi-scale geochemical mapping in China: Geochemistry: Exploration, Environment, Analysis, v. 8, p. 333–341, doi:10.1144/1467-7873/08-184.

Xuejing, X., Xuzhan, M., and Tianxiang, R., 1997, Geochemical mapping in China: Journal of Geochemical Exploration, v. 60, p. 99–113, doi:https://doi.org/10.1016/S0375-6742(97)00029-0.

Yilmaz, H., Sonmez, F.N., and Carranza, E.J.M., 2015, Discovery of Au–Ag mineralization by stream sediment and soil geochemical exploration in metamorphic terrain in western Turkey: Journal of Geochemical Exploration, v. 158, p. 55–73, doi:https://doi.org/10.1016/j.gexplo.2015.07.003.

Zuo, R., Wang, J., Xiong, Y., and Wang, Z., 2021, The processing methods of geochemical exploration data: past, present, and future: Applied Geochemistry, v. 132, p. 105072, doi:https://doi.org/10.1016/j.apgeochem.2021.105072.

10 Figures

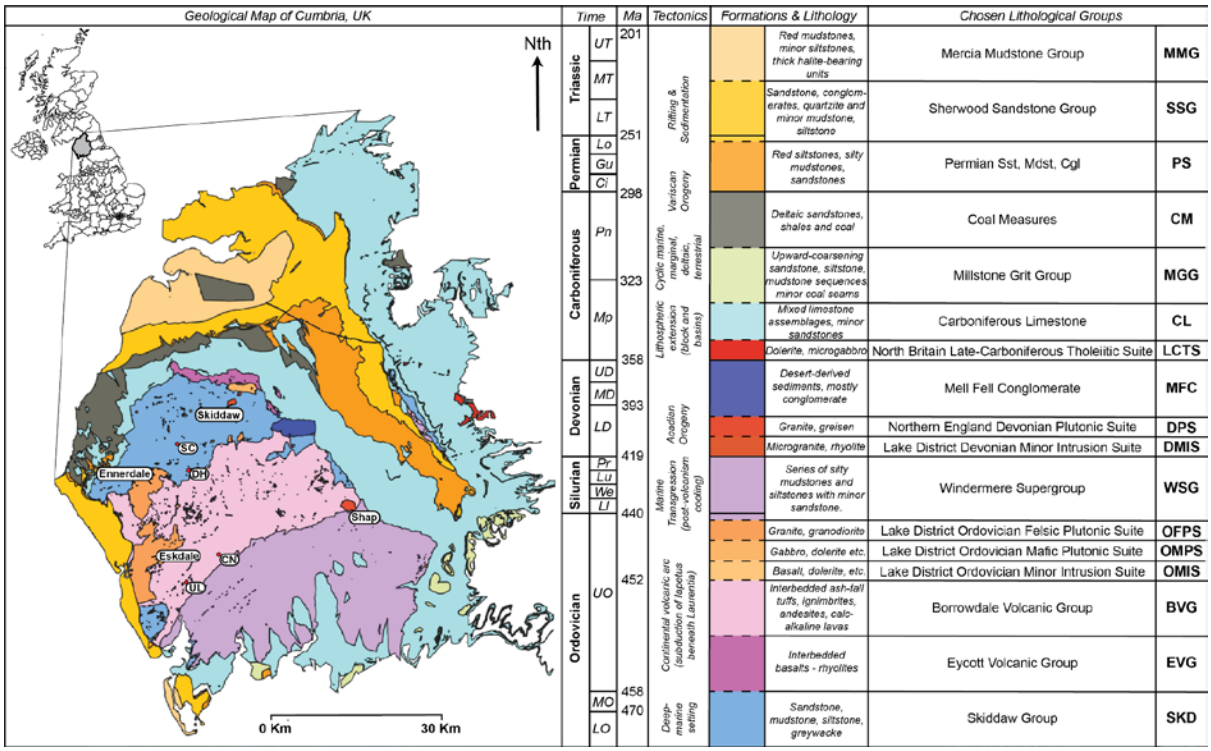

Figure 1: *Regional scale, geological map of Cumbria with classified lithological formations and groups (adapted from British Geological Survey 50k geological map (Brown. 1980)). A simplified chronostratigraphic diagram is presented to describe the key lithological and tectonic changes through the area and general lithologies per Group, starting from the Lower Ordovician and ending in the Upper Triassic. Abbreviated names for each Group and significant intrusions are labelled on the map to aid reference from the text. Known As-Co-Cu-Ni mineralisation is labelled: SC - Scar Crags, DH - Dale Head North, CN - Coniston area (including Seathwaite), UL - Ulpha.*

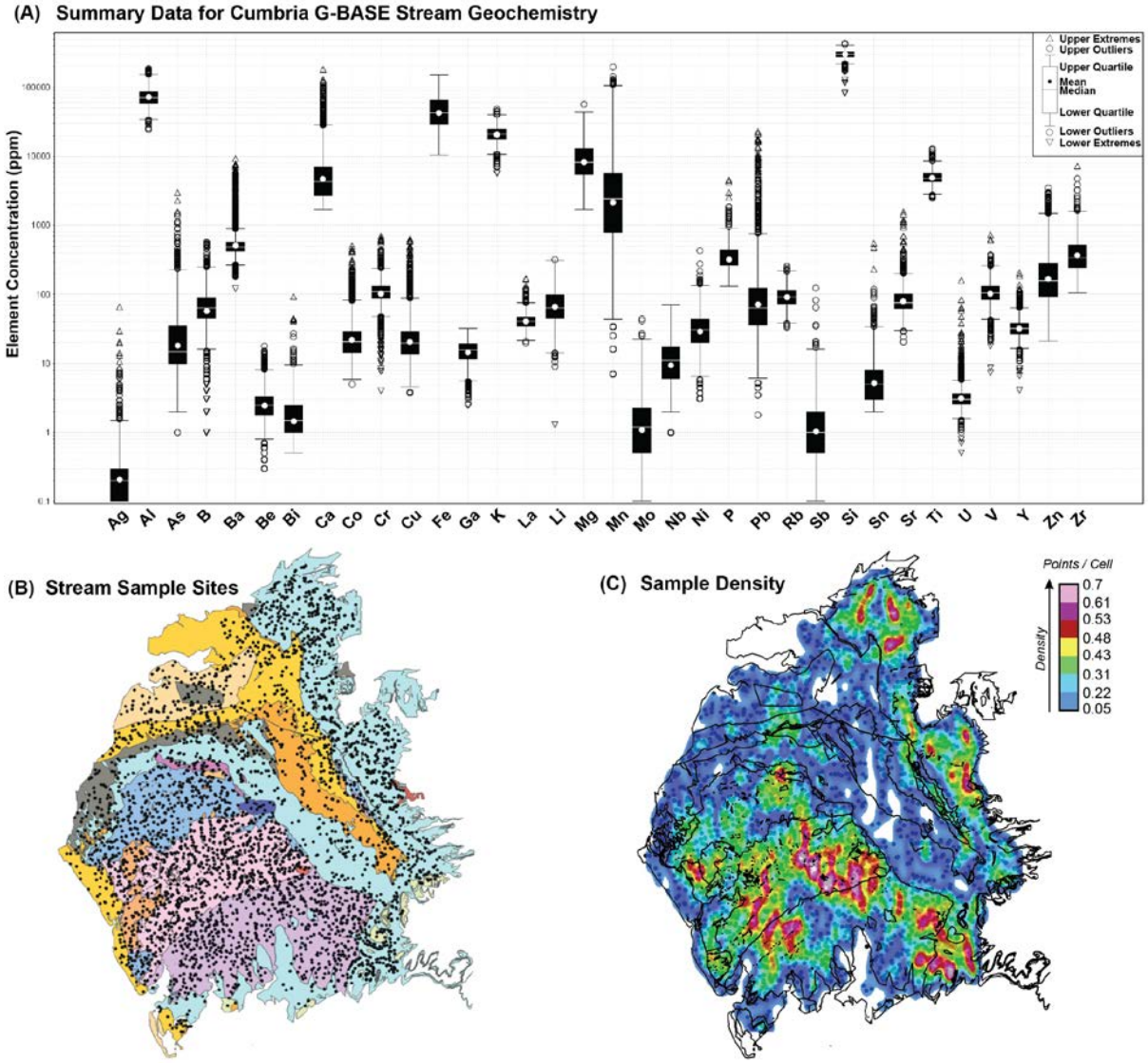

Figure 2: *(A) Box and Whisker plot for stream sediment element data used in this study; (B) locations for all 3974 stream sediment sample collection points within Cumbria, relative to 50k scale geological map; (C) the relative density of these data points with overlain geological boundaries. For geological formation and group names in (B) refer to Figure 1.*

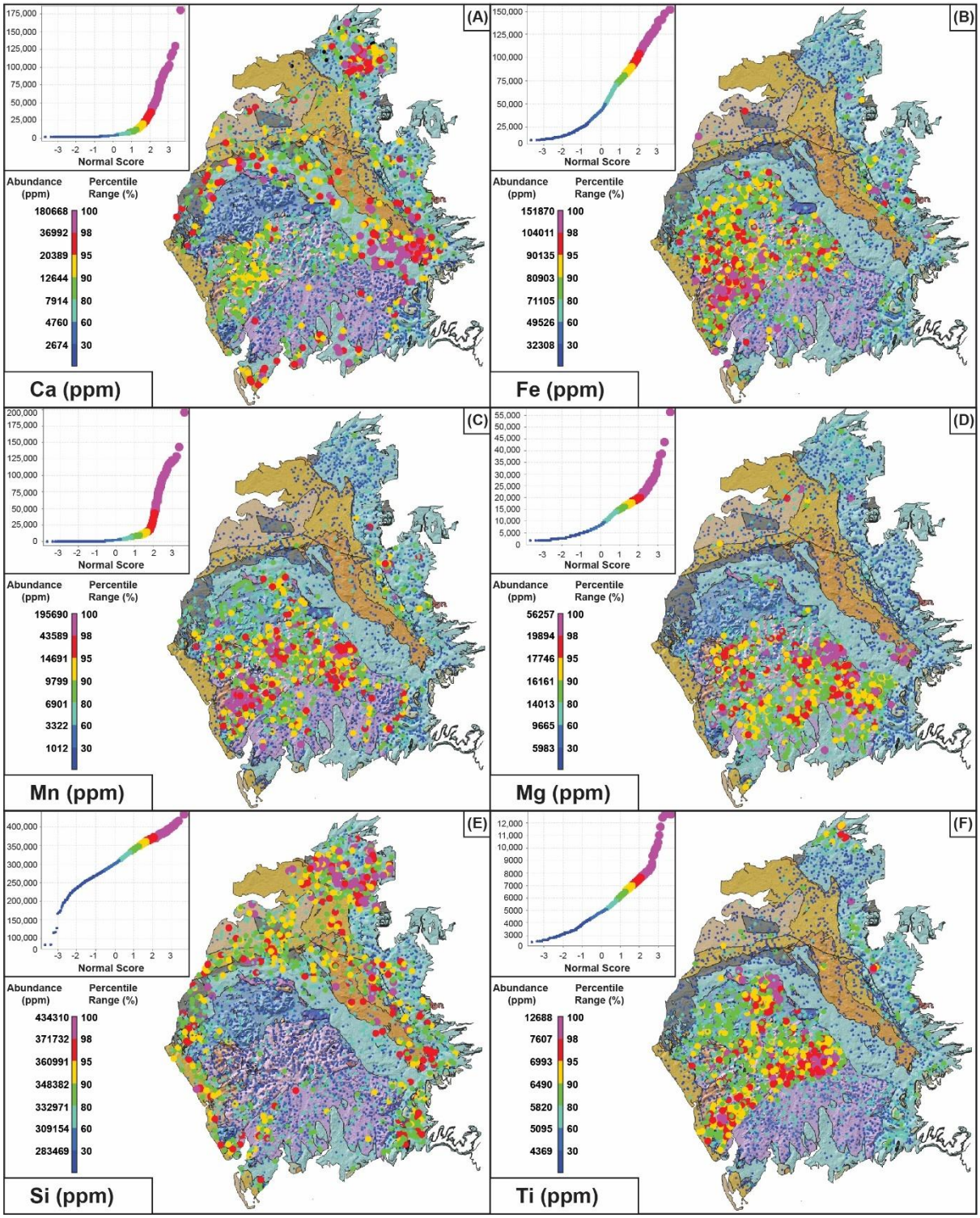

***Figure 3**: Major element concentrations in stream sediments across Cumbria. Data with 0 values have been excluded to better highlight higher concentration anomalies. For geological formation and group names refer to Figure 1.*

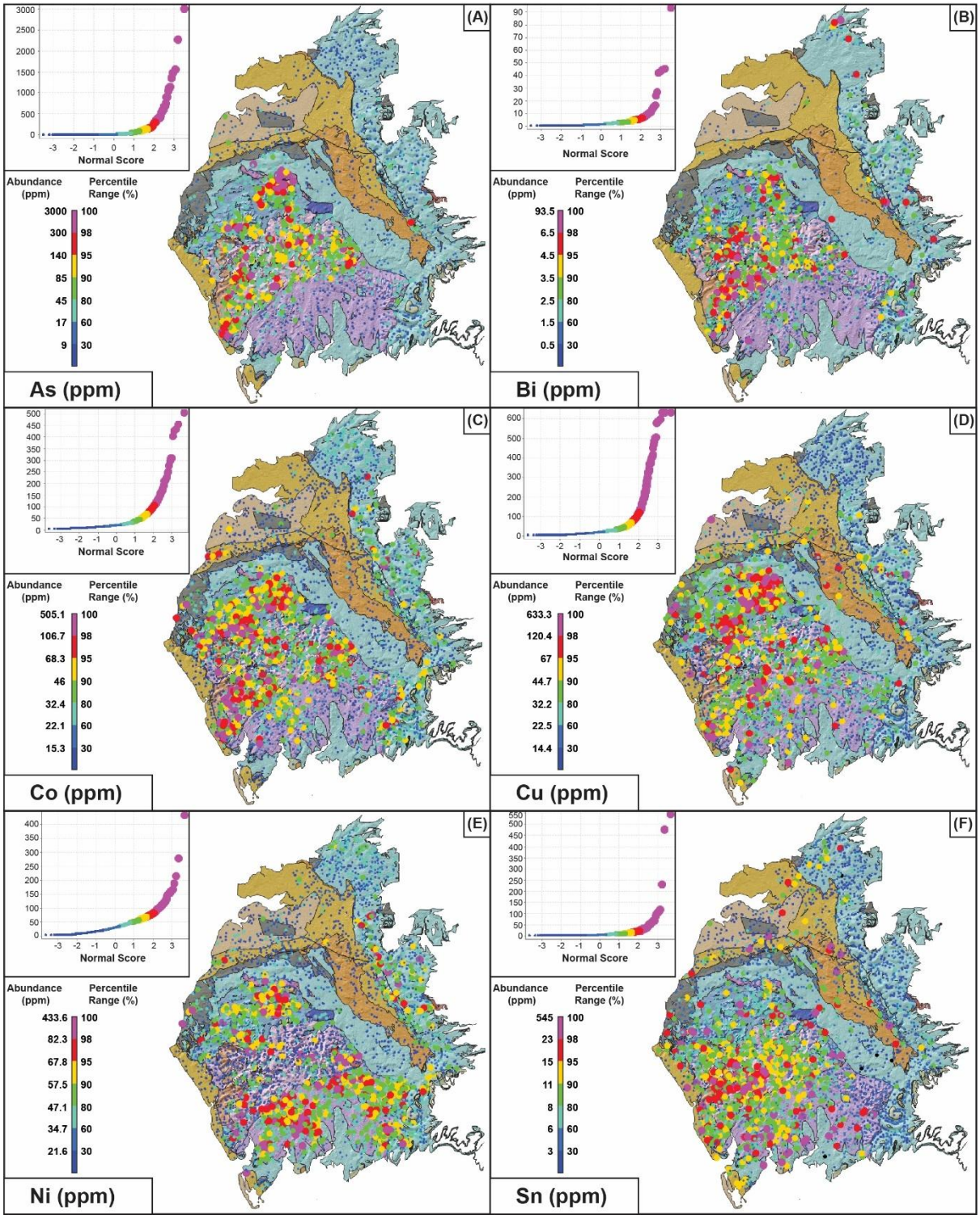

***Figure 4**: Ore-related element concentrations in stream sediments across Cumbria. Data with 0 values have been excluded to better highlight higher concentration anomalies. For geological formation and group names refer to Figure 1.*

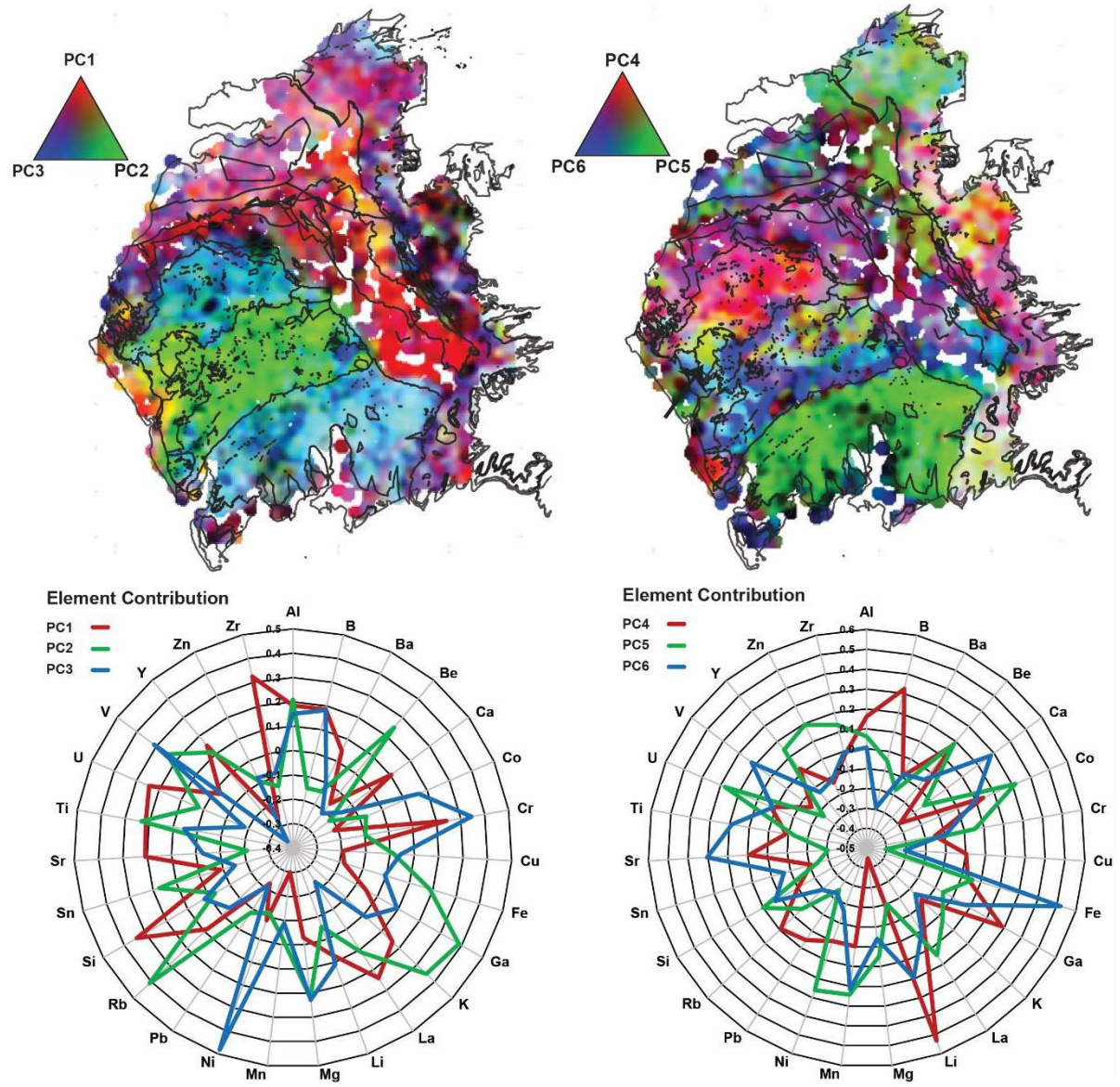

Figure 5: *RGB map showing the results of PC1-3 and PC4-6, with geological linework overlayed. Geochemical contributions to each principal component are outlined below the maps to show elemental variation and grouping. PC1-3 defines the geological boundaries for the BVG (green), SKD and WSG (blue), and Carboniferous-Jurassic groups (red-purple). PC4-6 disaggregates the SKD (pink - red) from the WSG (green), with more definition of the Ennerdale (yellow) and Shap granites (red).*

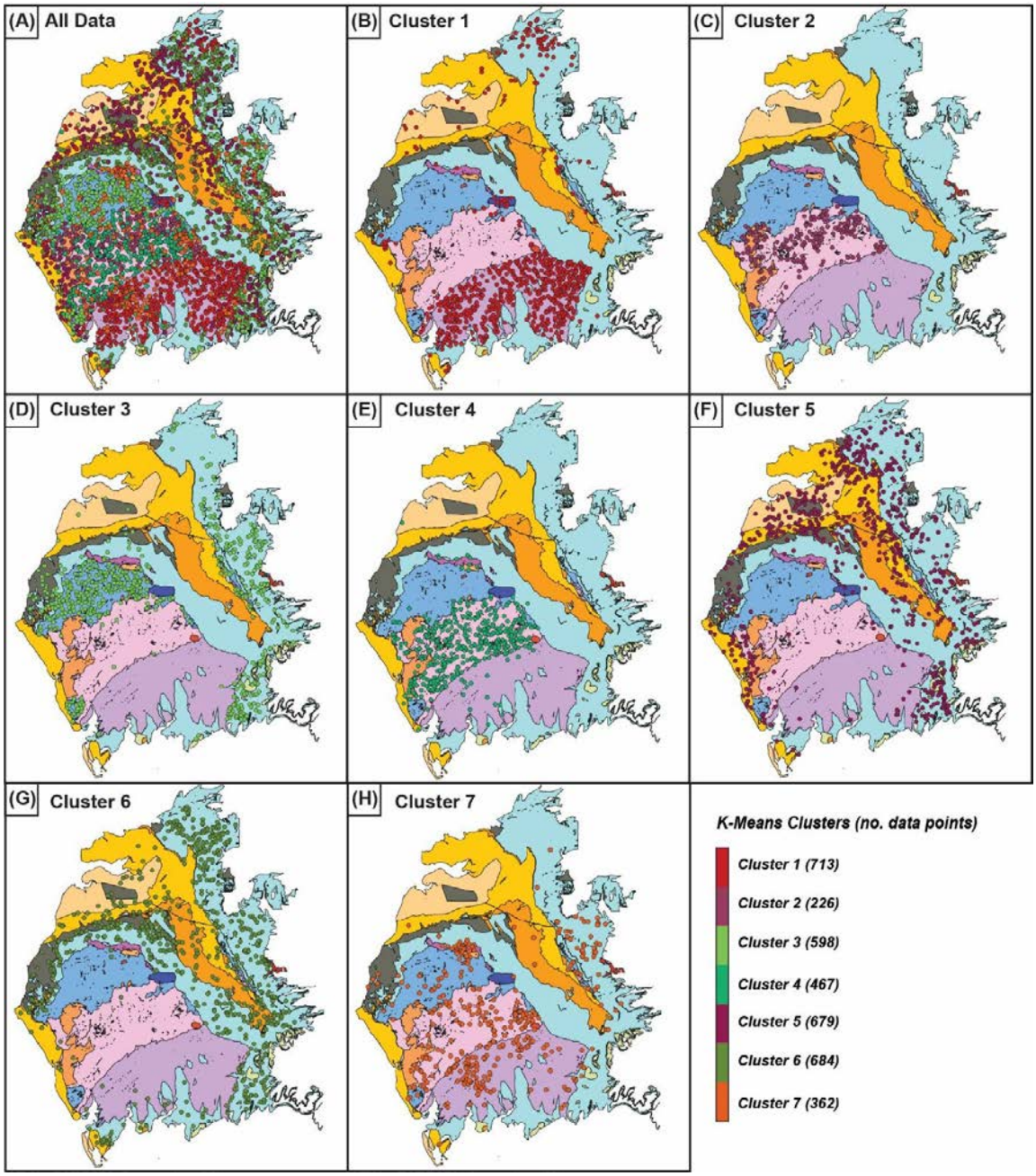

***Figure 6**: K-means clustering results projected over 50k geological boundaries in Cumbria. (A) All K-means cluster results; (B) isolated cluster 1 results (713 points), 74.57 % of which are concentrated in the WSG boundary, and 14 % in the northern Carboniferous Limestone; (C) isolated cluster 2 results (226 points), 73.01 % of which is concentrated in the BVG, and 19.03 % in the Ordovician Felsic Plutonic Suite (specifically the Ennerdale granodiorite and northern edges of the Eskdale granite); (D) isolated cluster 3 (598 points), 47.83 % of which is concentrated in the SKD, and 39.13 % in the Carboniferous Limestone; (E) isolated cluster 4 (467 points), 80.09 % of which is concentrated in the BVG; (F) isolated cluster 5 (679 points), 40.94 % of which is concentrated in the Carboniferous Limestone, 27.25 % in the Sherwood Sandstone, and 8.39 % in both the Permian sediments and Mercia Mudstone Group; (G) isolated cluster 6 (684 points), 63.16 % of which concentrates in the Carboniferous Limestone, and 9.06 % in the Sherwood Sandstone; (H) isolated cluster 7 (362 points), 31.49 % of which concentrates in the Eycott Volcanic Group, 27.62 % in the BVG, 16.02 % in the Carboniferous Limestones, and 12.98 % in the SKD.*

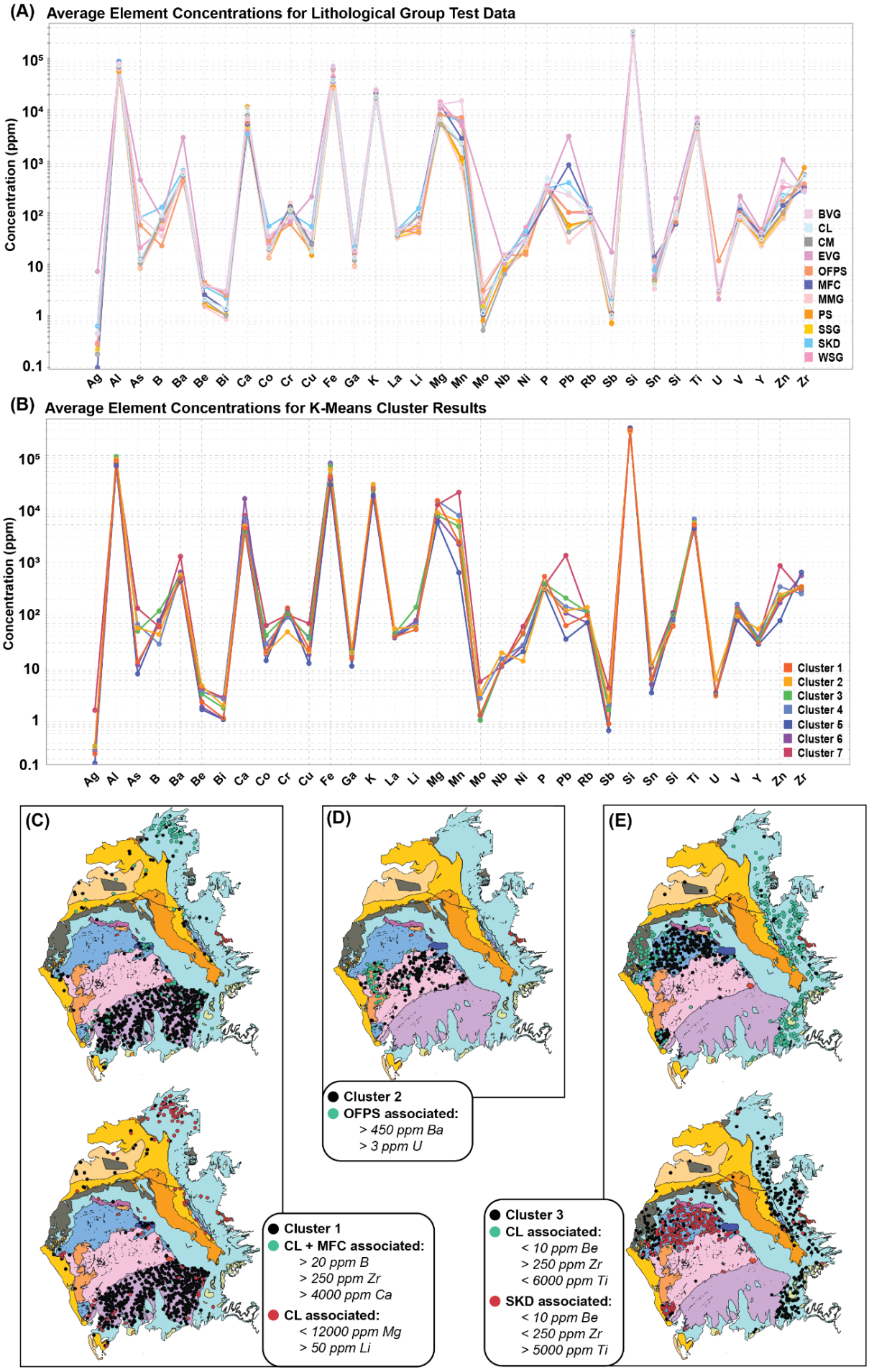
(A) Average Element Concentrations for Lithological Group Test Data
Concentration (ppm)
BVG
CL
CM
EVG
OFPS
MFC
MMG
PS
SSG
SKD
WSG
(B) Average Element Concentrations for K-Means Cluster Results
Concentration (ppm)
Cluster 1
Cluster 2
Cluster 3
Cluster 4
Cluster 5
Cluster 6
Cluster 7
(C)
(D)
(E)
Cluster 2
OFPS associated:
> 450 ppm Ba
> 3 ppm U
Cluster 1
CL + MFC associated:
> 20 ppm B
> 250 ppm Zr
> 4000 ppm Ca
CL associated:
< 12000 ppm Mg
> 50 ppm Li
Cluster 3
CL associated:
< 10 ppm Be
> 250 ppm Zr
< 6000 ppm Ti
SKD associated:
< 10 ppm Be
< 250 ppm Zr
> 5000 ppm Ti

Figure 7: *(A) average geochemistry for lithology test data; (B) average geochemistry for cluster results 1-7; (C-E) disaggregation of K-means clusters 1 (C), 2 (D) and 3 (E) using manually identified geochemical ranges. Only lithological formations or groups that have >5 % contribution to clusters 1, 2 or 3, or are able to be disaggregated using geochemistry are shown on the parallel coordinate plots to aid visibility of key data. Cluster 1 has been disaggregated into separate WSG, CL + MFC, and CL components using B, Zr, Ca, Mg, and Li values. From within cluster 2 OFPS-associated components have been isolated using Ba and U values. From cluster 3 CL and SKD associated components have been isolated using Be, Zr, and Ti values. The OFPS were depleted in Cu and enriched in U but remained relatively similar to the cluster 4 averages for the remaining elements. The BVG is higher in Mn and Zn than the OFPS and cluster 4 average. The CL was higher in P, Pb and Zn than the cluster 5 average, whilst the PS were only higher in Ca, with the remaining elements at similar concentrations. The SSG was lower in Pb than the cluster 6 average, whilst the CL were higher in P and Pb; however, the remaining elements were very similar and so was not possible to successfully distinguish these further. The SKD was higher in B and Li comparatively to the cluster 7 average, and lower in Mg, Pb and Zn. The BVG was lower in B, Cu, Pb and Zn than cluster 7 but remained relatively similar overall. The EVG were higher in As, Ba, Cu, Pb and V as well as lower in U. Despite these element differences in clusters 4-7, there is not enough to provide distinct disaggregation of the lithological groups like in clusters 1-3.*

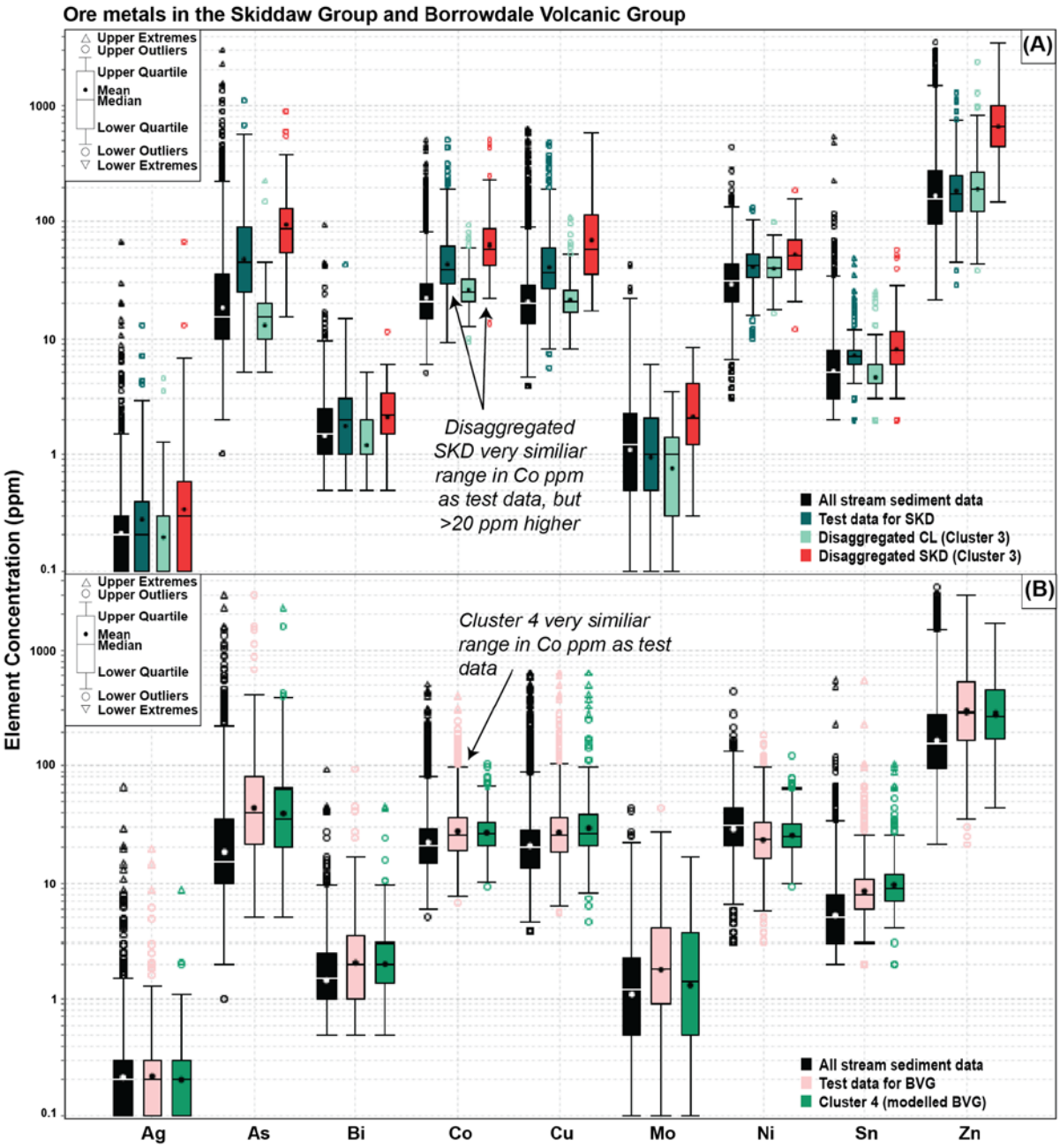

***Figure 8**: (A) Average ore metal lithogeochemistry for the SKD test data, disaggregated carbonate-associated data and SKD-associated data from within cluster 3; (B) Average ore metal lithogeochemistry for the BVG test data and cluster 4 data. Average metal lithogeochemistry for the total G-BASE data set is also shown in both panels for comparison. Cluster 3 (disaggregated SKD) has an average Co value of 63.26 ppm, almost double the SKD test data value (39 ppm), therefore we have identified a higher Co average within the SKD than expected. Here As, Cu, Mo, and Zn mean values are also notably higher than the test data. Cluster 4 (representing the BVG) has an average Co value of 26.86 ppm, almost identical to the BVG test data, as are the mean values for the remaining ore elements presented, indicating expected results were met successfully.*

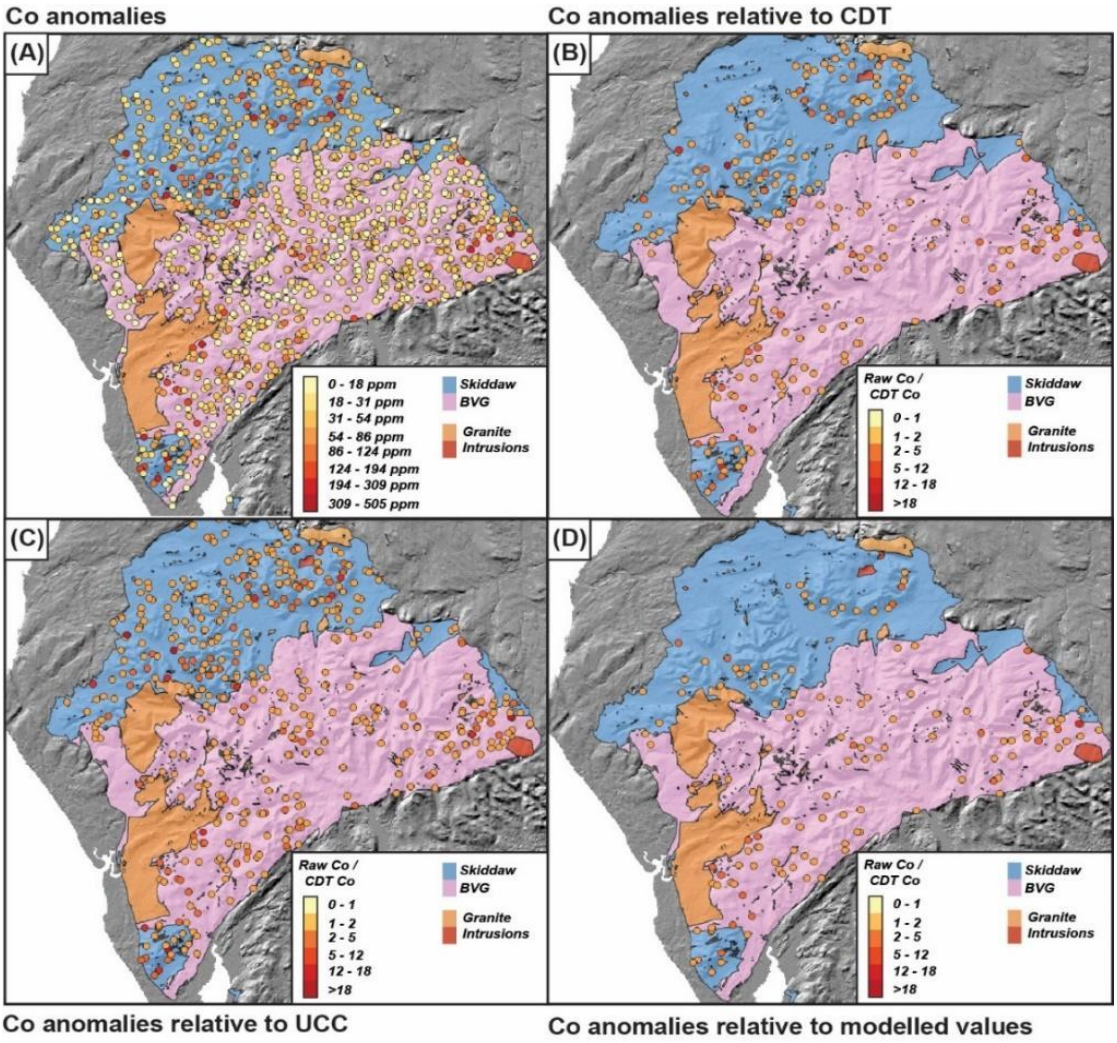

***Figure 9**: Anomalies of Co in G-BASE stream sediment data relative to (A) raw data; (B) average continental crust (CDT); (C) average upper continental crust (UCC); (D) modelled averages for the SKD and BVG from this study. In box D, data points within the Skiddaw are normalised to SKD-associated average cobalt (63.26 ppm) disaggregated from cluster 3, and data within the BVG is normalised to cluster 4 average cobalt (26.86 ppm). The number of data points indicating anomalies of Co decreased from the raw data to the CDT, UCC and then finally to the cluster results, indicating that using the cluster results as an enrichment baseline makes it easier to identify 'true' anomalies as more data is filtered out by the higher average Co values for the SKD and BVG lithologies. Anomalies are evenly distributed across the SKD and BVG, although those in the SKD will have higher Co concentrations as they are being compared to the higher SKD Co average.*

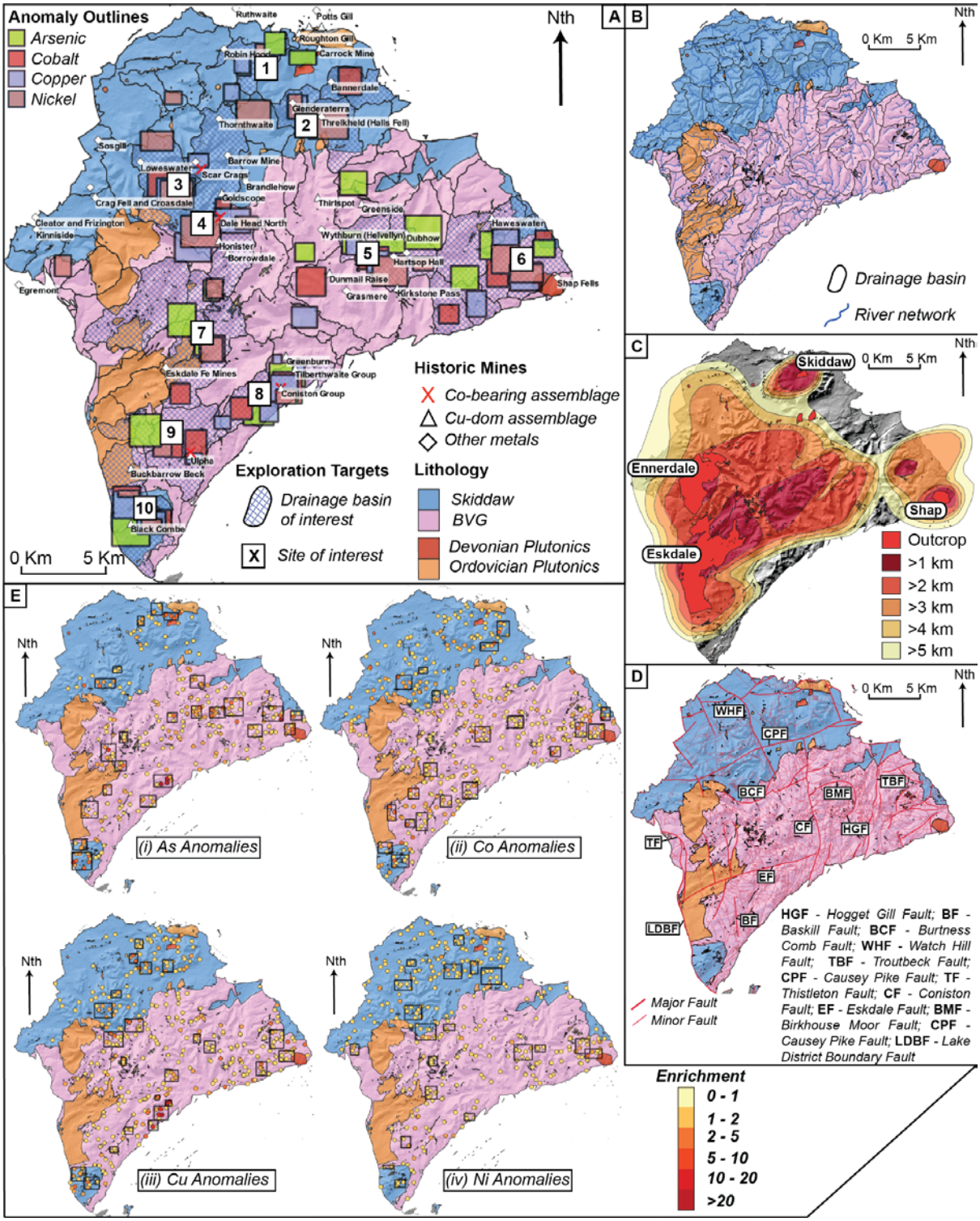

Figure 10: *(A) 10 identified areas of prospective As-Co-Cu-Ni mineralisation across the Skiddaw Group (blue) and Borrowdale Volcanic Group (pink), the criteria for these based on proximity to historic mining sites and criteria in the other map panels: (B) clustering of enrichments within same river catchments; (C) proximity to intrusive bodies at depth or outcrop; (D) proximity to faults / structures; (E) anomaly maps for (i) As, (ii) Co, (iii) Cu, (iv) Ni. Five prospective areas are in the SKD and five in the BVG, with sites 3, 4, 8, and 9 close to known As-Co-Cu-Ni mineralisation at Scar Crags, Dale Head North, Seathwaite, and Ulpha.*

11 Tables

Table 1: *Categorised list of elements used in this study, from the Cumbria G-BASE stream sediment dataset.*

Description	Elements
Removed due to poor data availability (total 21)	*Br, Ce, Cl, Cs, Ge, Hf, Hg, I, In, Na, Nd, S, Se, Sc, Sm, Ta, Te, Th, Tl, W, Yb*
Removed due to significant data quality issues (total 1)	*Cd*
Elements used in study (total 34)	*Ag, Al, As, B, Ba, Be, Bi, Ca, Co, Cr, Cu, Fe, Ga, K, La, Li, Mg, Mn, Mo, Nb, Ni, P, Pb, Rb, Sb, Si, Sn, Sr, Ti, U, V, Y, Zn, Zr*
Elements used in principal component analysis and K-means clustering (total 27)	*Al, B, Ba, Be, Ca, Co, Cr, Cu, Fe, Ga, K, La, Li, Mg, Mn, Ni, Pb, Rb, Si, Sn, Sr, Ti, U, V, Y, Zn, Zr*

Table 2: *Proportional overlap of each lithological group (test data) by each K-means cluster result. Data presented is percentage (%).*

Lithological Groups		Cluster 1	Cluster 2	Cluster 3	Cluster 4	Cluster 5	Cluster 6	Cluster 7	Unconsidered
Ordovician - Triassic Sediments									
	SKD	2.51	3.26	71.68	5.01	2.51	2.76	11.78	0.5
	WSG	73.85	0.14	1.39	3.2	2.09	2.64	15.86	0.83
	MFC	75	-	-	-	16.67	-	8.33	-
	CL	8.45	-	19.78	0.51	23.5	36.52	4.9	6.34
	MGG	-	-	21.43	-	42.86	14.29	-	21.43
	CM	0.76	-	18.94	-	29.55	46.21	3.03	1.52
	PS	2.24	-	2.99	-	42.54	46.27	2.24	3.73
	SSG	6.81	0.31	4.02	0.93	57.28	18.89	0.93	10.84
	MMG	9.82	-	1.79	0.89	50.89	17.86	-	18.75
Ordovician Volcanics									
	EVG	-	-	3.7	11.11	-	7.41	77.78	-
	BVG	2.86	21.48	1.56	48.7	2.08	0.39	13.02	9.9
Ordovician - Permian Intrusives									
	OMIS	10	-	20	50	10	-	10	-
	OMPS	-	-	16.67	33.33	-	-	50	-
	OFPS	0.96	41.35	-	26.92	9.62	0.96	3.85	-
	DMIS	33.33	-	-	33.33	-	-	33.33	-
	DPS	-	42.86	42.86	14.29	-	-	-	-
	LCTS	-	-	10	-	10	50	10	20
	Error	9.09	-	9.09	-	18.18	45.45	9.09	9.09

Table 3: *Prospective areas of interest identified using the model results of this study, combined with other typical exploration-related factors (historic mining, geological structures, proximity to known ore-hosting lithology, number of drainage catchments, and batholith topography). Points are assigned relative to these factors to assess prospectivity ranking; low areas =< 4 points, medium areas 4-8 points, high areas >8 points. Sites are listed in order from the map (Figure 10), not in order of prospectivity.*

Area of Interest	Indicative Criteria	Points	Ranking
(1) Bassenthwaite	Overlapping As-Cu-Ni anomalies; within 1 catchment; relatively shallow batholith topography (close to Skiddaw granite); hosted in SKD; historic mining present.	9	High
(2) Threlkeld	Overlapping Co-Ni anomalies; within 1 catchment; deeper batholith topography but relatively close to Skiddaw granites; hosted in SKD; historic mining present.	7	Medium
(3) Crummock Water	Overlapping As-Cu-Co-Ni anomalies; within 1 catchment; relatively shallow batholith topography (close to Ennerdale granite); hosted in SKD.	11	High
(4) Dale Head North / Honister	Overlapping Co-Cu-Ni anomalies; within 2 catchments; relatively shallow batholith topography (close to Ennerdale granite); hosted in BVG / SKD boundary; historic mining present.	10	High
(5) Hartsop	Overlapping As-Cu-Co-Ni anomalies; within 1 catchment; moderate batholith topography; hosted in BVG; historic mining present.	11	High
(6) Keld / Shap	Overlapping Co-Cu-Ni anomalies; within 2 catchments; relatively shallow batholith topography (near Shap granite); hosted in BVG.	9	High
(7) Hard Knott / Great How	Overlapping As-Co-Ni anomalies; within 1 catchment; within 1km batholith topography (close to Eskdale granite); regional (Eskdale Fault) and local scale structures; hosted in BVG.	11	High
(8) Coniston / Seathwaite / Tilberthwaite	Overlapping As-Cu-Co-Ni anomalies; within 1 catchment; relatively deeper batholith topography; regional (Coniston Fault) and local scale structures; hosted in BVG; historic mining present.	10	High
(9) Devoke Water / Ulpha	Overlapping As-Co-Ni anomalies; within 2 catchments; moderately shallow batholith topography (close to Eskdale granite); regional (Baskill Fault) and local scale structures; hosted in BVG; historic mining present.	10	High
(10) Black Combe	Overlapping As-Co-Cu-Ni anomalies; within 2 catchments; deeper batholith topography; local structures; hosted in SKD; historic mining present.	8	High

1. Appendix A - Test Data

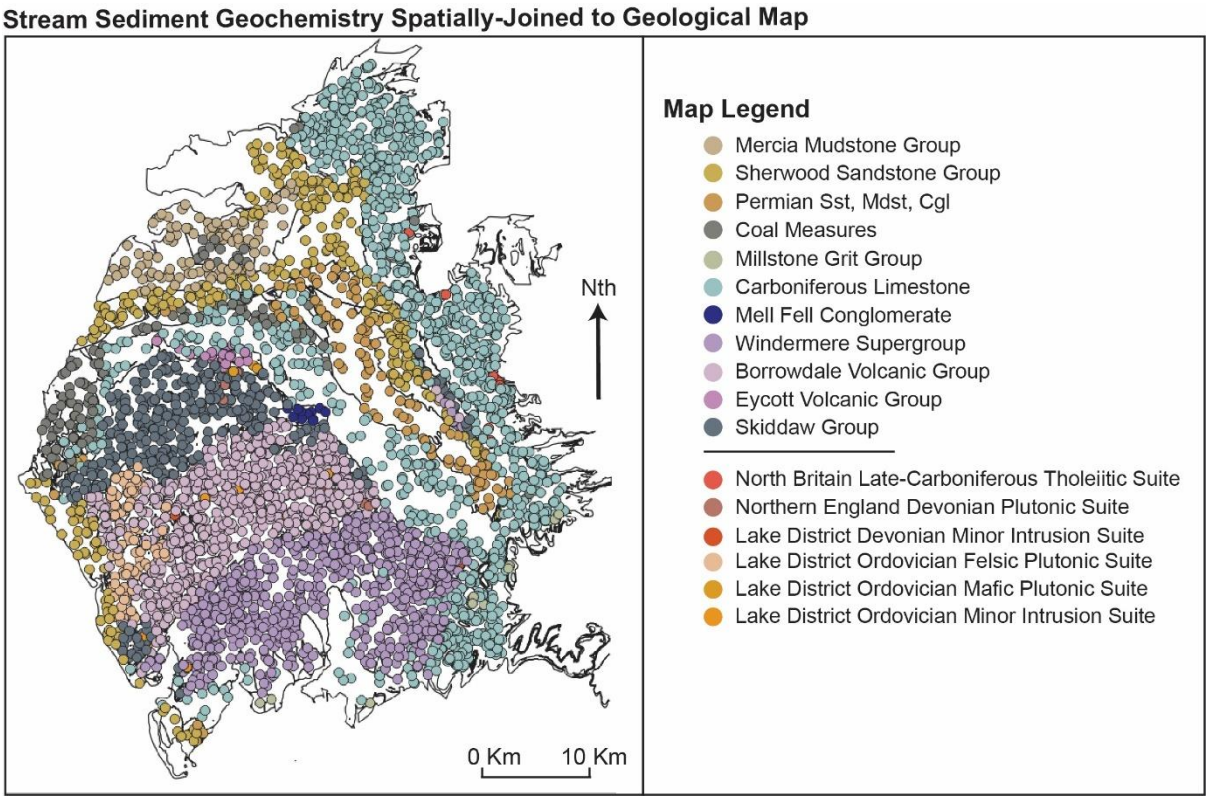

***Figure A1**: Spatially joined G-BASE stream sediment data (points) and BGS 50k geological map (vector line work). This combined data represented 'realistic' chemistries for the Lake District groups, as comparative test data for this study.*

Appendix B - Principal Component Analysis Results

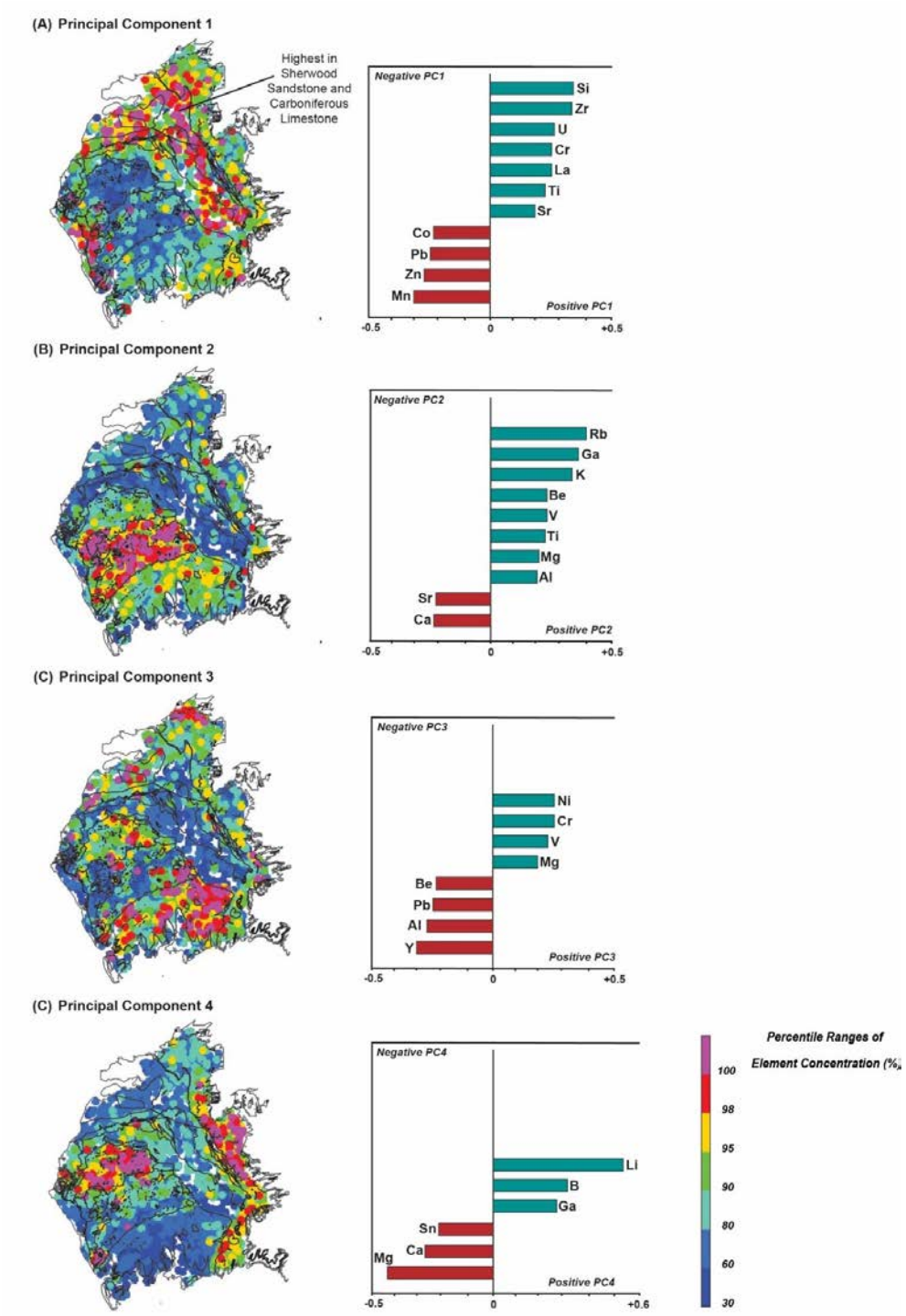

Figure B1: *Maps of principal component results, showing variation in eigenvalues within each principal component 1-4. (A) Principal component 1 highlighting Mn, Pb, Zn and Co within the Sherwood Sandstones and Carboniferous Limestone and Sr, Ti La, Cr, U, Zr, Si in the SKD and BVG; (B) Principal component 2 highlighting Ca and Sr within the BVG, and Al, Mg, Ti, V, Be, K, Ga and Rb in the Permian - Jurassic formations; (C) Principal component 3 highlighting Y, Al, Pb and Be predominantly within the WSG, SKD, and Mg, V, Cr, and Ni in the BVG, Ordovician intrusives and carbonates; (D) Principal component 4 highlighting Mg, Ca and Sn within the SKD and Carboniferous Limestone, and Ga, B and Li in the remaining formations.*

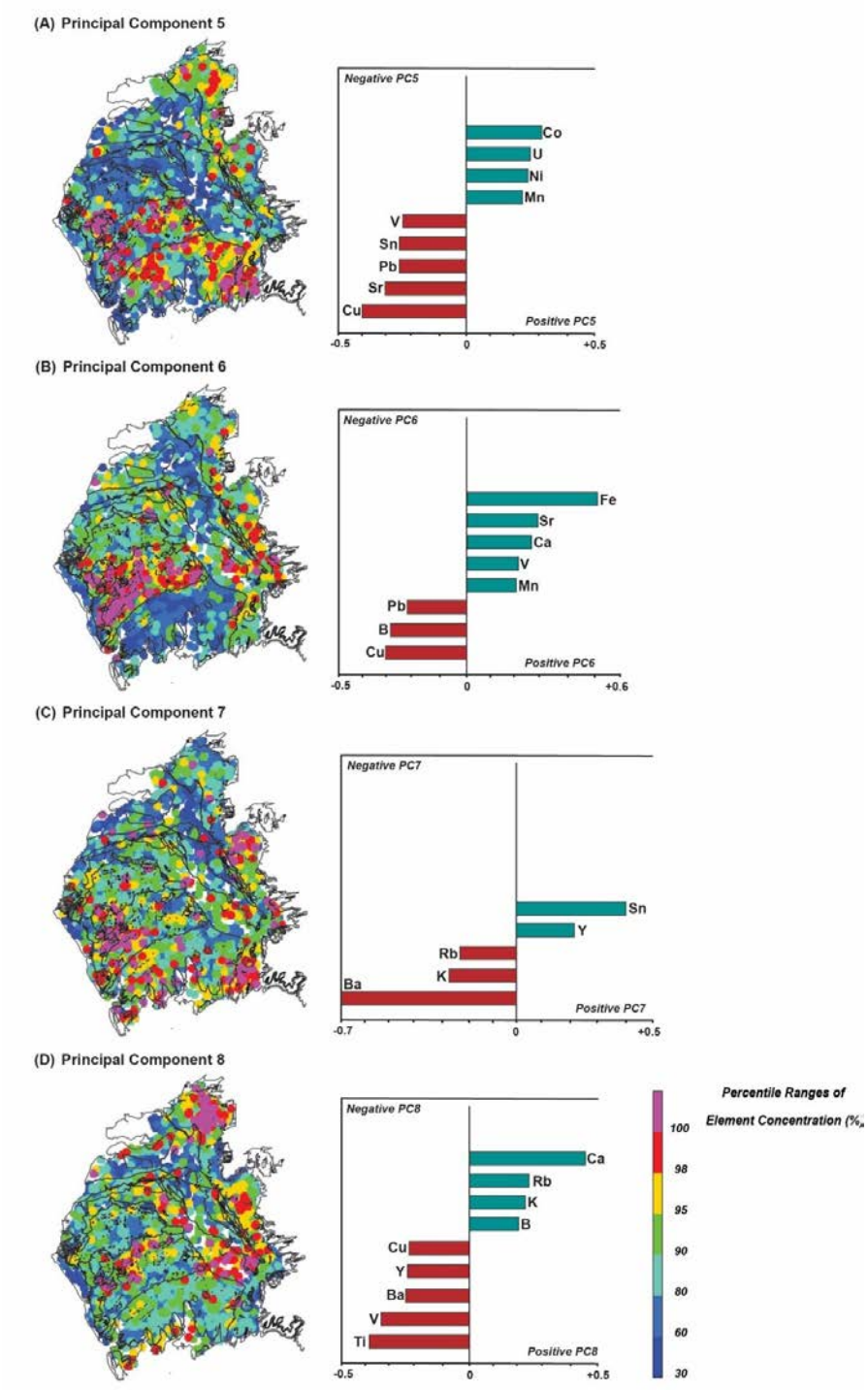

Figure B2: *Maps of principal component results, showing variation in eigenvalues within each principal component 5-8. (A) Principal component 5 highlighting Cu, Sr, Pb, Sn, and V sporadically across the WSG, Ordovician intrusives, BVG and Carboniferous limestone, and Mn, Ni, U, Co in the SKD and Permian sediments; (B) Principal component 6 highlighting Cu, B and Pb within the BVG, and Mn, V, Ca, Sr and Fe in the SKD and Permian - Jurassic formations; (C) Principal component 7 highlighting Ba, K, and Rb sporadically in the BVG and carbonates, and Y and Sn in the Sherwood Sandstone; (D) Principal component 4 highlighting Ti, V, Ba, Y and Cu within the northern Carboniferous Limestone, and B, K, Rb and Ca loosely in the Sherwood Sandstones.*

Appendix C - K Means Clustering Results

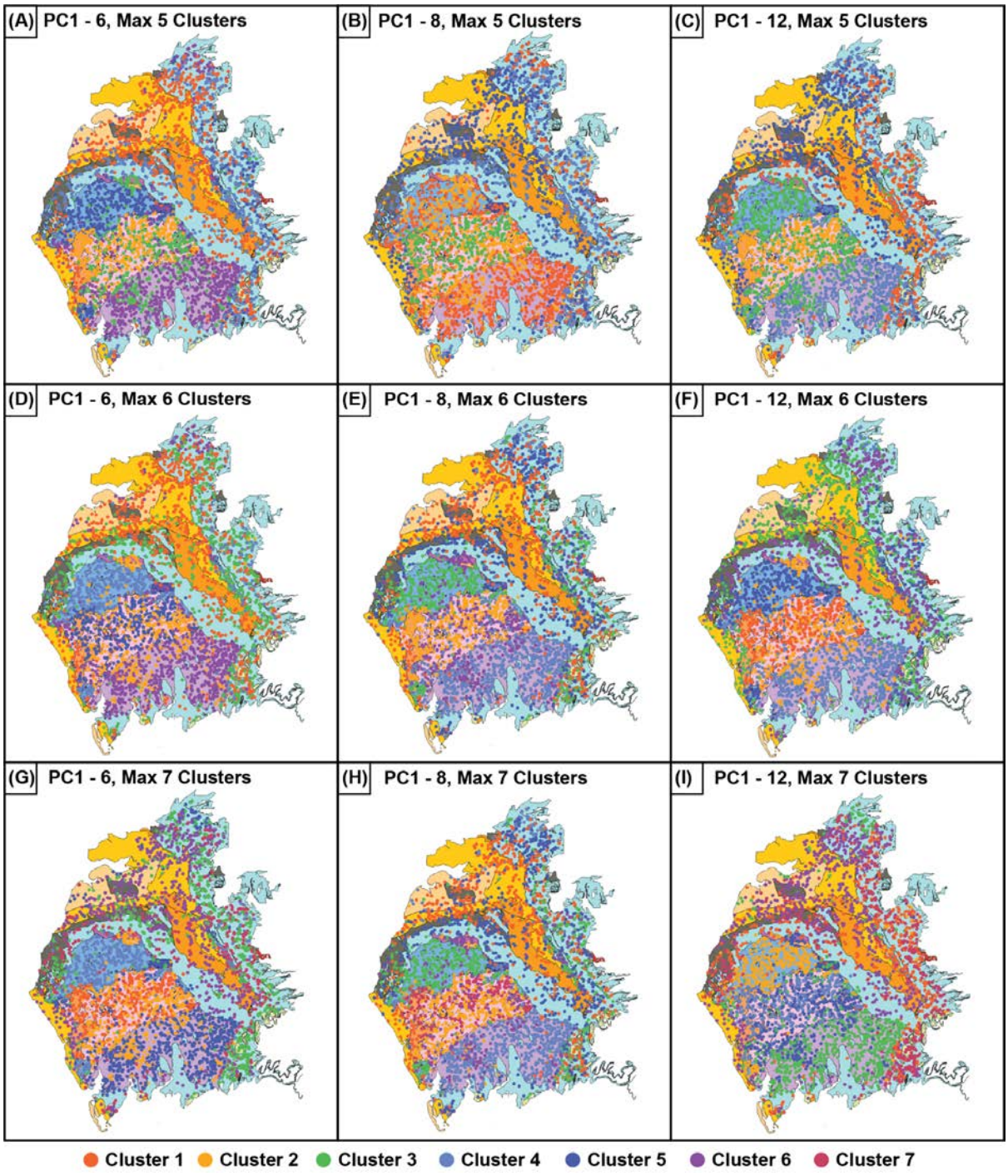

Figure C1: *K-means clustering results projected over 50k geological boundaries in Cumbria. (A, D, G) Experiment results using PC1-6 as input data, with maximum groupings of 5 (A), 6 (D) and 7 (G); (B, E, H) experiment results using PC1-8 as input data, with maximum groupings of 5 (B), 6 (E) and 7 (H); (C, F, I) experiment results using PC1-12 as input data, with maximum groupings of 5 (C), 6 (F and 7 (I). Results in (H) were used in this study for interpretation. Refer to Figure 1 for lithological group names.*

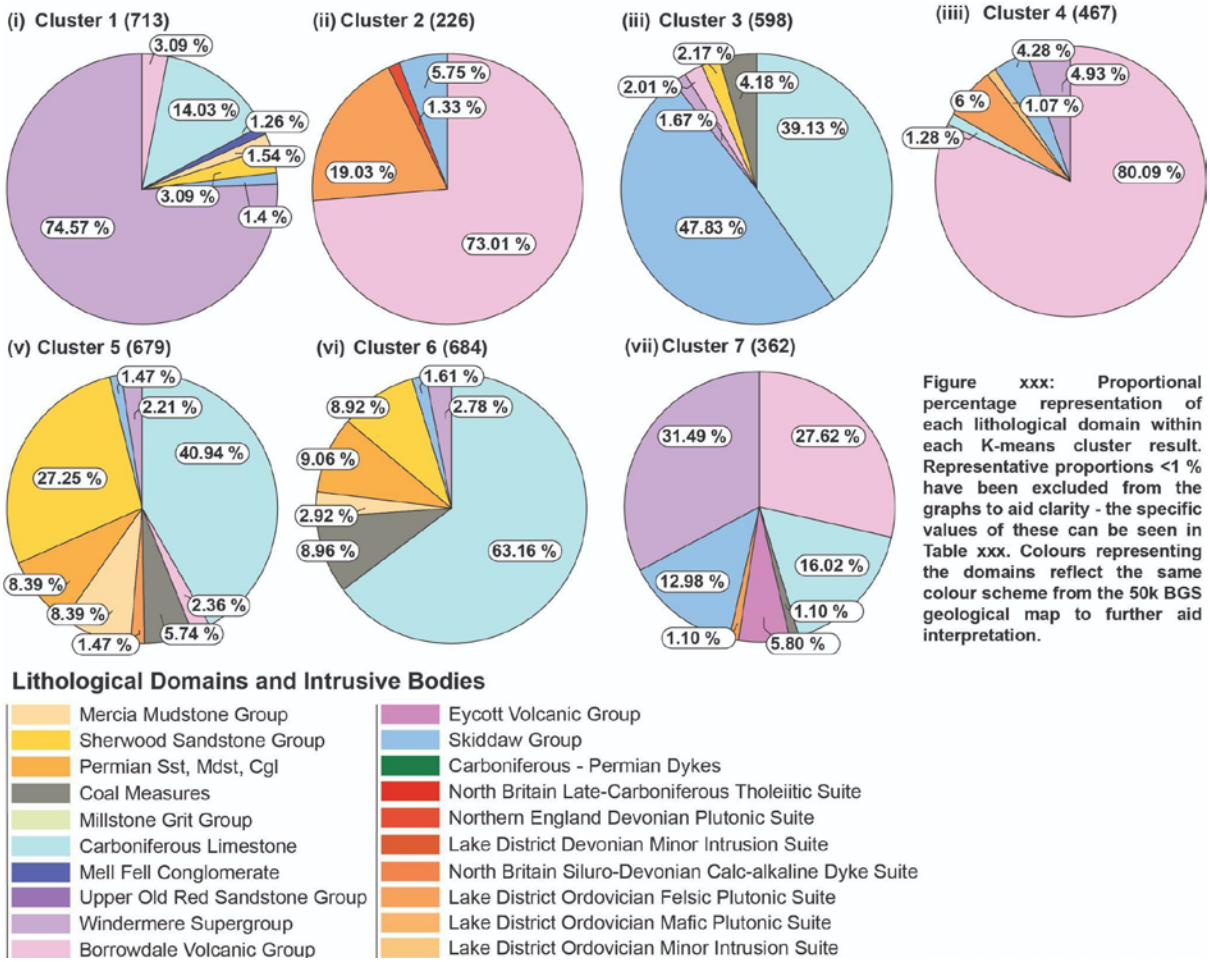

Figure xxx: Proportional percentage representation of each lithological domain within each K-means cluster result. Representative proportions <1 % have been excluded from the graphs to aid clarity - the specific values of these can be seen in Table xxx. Colours representing the domains reflect the same colour scheme from the 50k BGS geological map to further aid interpretation.

Figure C2: *Proportional percentage representation of each lithological formation and group within each K-means cluster result. Representative proportions <1 % have been excluded from the graphs to aid clarity.*

Appendix D - Workflow

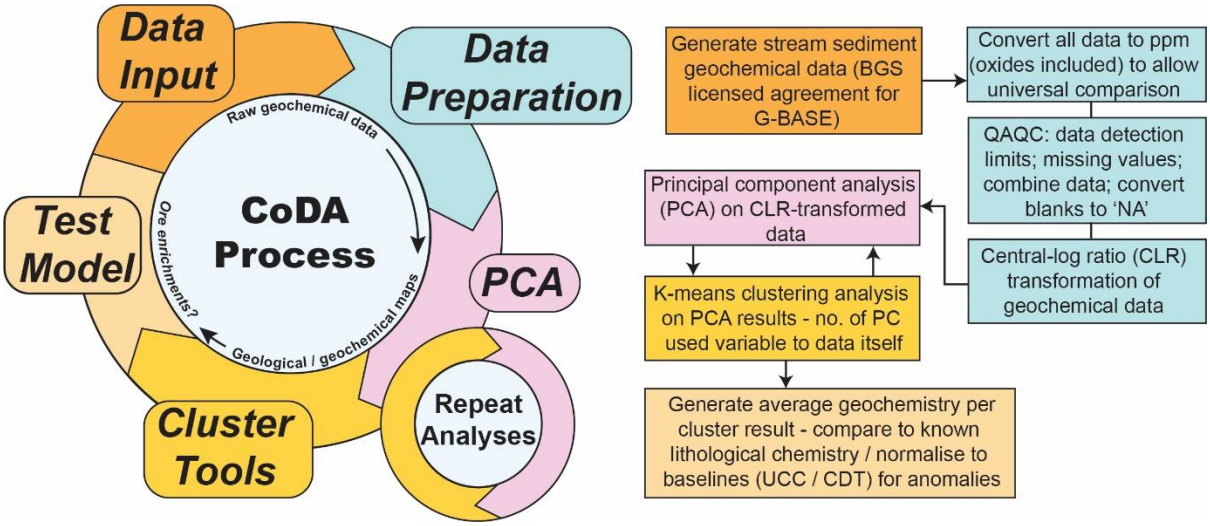

***Figure D1**: Generalised workflow used in this study to investigate stream geochemistry for use as a geological mapping tool, and mineral exploration tool.*